Journal of Umm Al-Qura University for Applied Science

journal homepage: https://uqu.edu.sa/en/jas/87823

Radiative atomic and collisional data for Ar VI allowed and forbidden lines

Haykel Elabidi

Common First Year Deanship, Physics Department, Umm Al-Qura University, Makkah, Saudi Arabia.[b]Laboratory of Molecular Spectroscopy and Dynamics, Sciences Faculty of Bizerte, Carthage University, Tunisia.

ARTICLE INFO

Article History:
Submission date: 17/11/2019
Accepted date: 16/11/2020

Keywords:
Atomic data, forbidden transitions, electron scattering, effective collision strengths.

ABSTRACT

Energy levels, lifetimes, oscillator strengths, radiative decay rates, line strengths, electron-impact collision strengths and effective collision strengths are presented for aluminium-like Ar VI. New radiative data for forbidden lines are presented for the first time. We used the following 12 configurations in our work: $3s^2 3p$, $3s3p^2$, $3s^2 3d$, $3p^3$, $3s3p3d$, $3s^2 4s$, $3s^2 4p$, $3p^2 3d$, $3s^2 4d$, $3s3p4s$, $3s3p4p$ and $3s3p4d$ yielding to 121 fine structure levels. The calculations have been carried out using the AUTOSTRUCTURE code. It included the one–body and the two–body (fine and non–fine structure) interactions of the Breit–Pauli Hamiltonian. No results for forbidden transitions have been found in the literature. For the collisional problem, the distorted wave approximation has been assumed. Collision strengths have been calculated at six electron energies: 10, 50, 100, 200, 400 and 800 Ry. Convergence of collision strengths with total angular momentum has been studied at each electron energy. For some lines, we make use also of the codes SUPERSTRUCTURE/DISTORTED WAVE/JAJOM to compare with the AUTOSTRUCTURE results. Effective collision strengths have been calculated for a wide range of temperatures up to 3.6×10^5 K, and are compared to those from the Breit–Pauli R–matrix method.

1. Introduction

Radiative atomic and collisional data have an important role in modelling of astrophysical plasmas and in tokamaks. In the case of non-local thermodynamic equilibrium (NLTE) plasmas, it is important to know all the excitation/ de-excitation processes that contribute to the intensity of the lines. Consequently, electron collision strengths are required for calculating level populations and spectral line intensities. These parameters can provide diagnostics of temperature, density, and abundance of elements in a plasma. Argon ions are important in astrophysics and in fusion [1,2]. The Ar VI absorption lines have been identified in the spectrum of a hydrogen-rich star LS V +46°21 [3]. These authors identified the Ar VI transition at 1303.87 Å as an isolated line in the HST/STIS (Space Telescope Imaging Spectrograph aboard the Hubble Space Telescope) spectrum of that star. It was the first time that Ar VI has been detected in the photosphere of any star. Excitation data for argon ions are also required to analyse data collected by spectrographs onboard other satellites, such as Chandra or XMM-Newton to be used as plasma diagnostics of stellar temperature and density.

The first results for the spectrum of Ar VI in the vacuum ultraviolet were published by Phillips and Parker [4]. A list of many theoretical and experimental works dedicated to the Ar VI ion before 1992 was reported in [5]. Recently, a new analysis of the Ar VI spectrum in the vacuum ultraviolet region was reported by Rainerie *et al.* [6], where adjusted and new energy levels and new classified lines were obtained. Calculations of energy levels, oscillator strengths and lifetimes have been performed by Gupta and Msezane [7] using only ten configurations. Newer calculations that provide oscillator strengths and transitions probabilities for Ar VI were presented in Froese Fischer *et al.* [8], where the authors used the multiconfiguration Hartree-Fock (MCHF) and the multiconfiguration Dirac-Hartree-Fock (MCDHF) methods. Electron-impact excitation calculations have been done for the argon isonuclear sequence using the first-order many-body perturbation theory [9] and using the Breit-Pauli R-matrix method [2]. The results of [2] have been provided as effective collision strengths. Some preliminary results for Ar VI have been presented in [10] (only for some transitions and without effective collision strengths). Here, we report a complete set of radiative atomic data (including for the first time forbidden transitions) and distorted wave collisional data: collision strengths and effective collision strengths for Ar VI.

We report in this work 121 Ar VI energy levels and compare them to the values compiled by the National Institute of Standards and Technology (NIST) [11] and to the newer existing theoretical results of Froese Fischer [8], where the MCHF method has been used. The radiative data (line strengths, absorption oscillator strengths and radiative decay rates) for electric dipole (E1) transitions involving the 121 levels have been compared to the MCHF resuts of [8]. Line strengths and radiative decay rates for electric quadrupole (E2) and octopole (E3) and magnetic dipole (M1) and quadrupole (M2) transitions have been calculated, since they are also required for plasma modelling. No data for forbidden lines have been found in the literature to perform comparisons. Additionally, theoretical lifetimes are listed for all the 121 obtained levels. Electron-impact excitation collision strengths at six electron energies 10, 50, 100, 200, 400 and 800 Ry have also been presented. The structure and collision calculations have been carried out using the AUTOSTRUCTURE code (AS) of Badnell [12,13]. We study the convergence of collision strengths with the total angular momentum, and we illustrate this for some transitions. In several cases, we perform scattering calculations using the University College London (UCL) codes: SUPERSTRUCTURE (SST) [14], DISTORTED WAVE (DW) [15] and JAJOM [16,17] and compare with the AS results. We present also effective collision strengths for large temperature range suitable for plasma modelling.

2. Description of the numerical method

2.1. Structure

The atomic structure has been calculated using the AS code of Badnell [12,13], by constructing target wavefunctions using radial wavefunctions calculated in a scaled Thomas–Fermi–Dirac–Amaldi statistical model potential. The scaling parameters λ_{nl} (depending on n and l) are determined by minimizing the sum of the energies of all the target terms, computed in LS coupling, i.e. neglecting all relativistic effects. In this code, besides the one–body and the two–body fine structure interactions, the two–body non–fine structure operators of the Breit–Pauli Hamiltonian, namely contact spin–spin,

* **Corresponding Author**
Common First Year Deanship, Physics Department, Umm Al-Qura University, Makkah, Saudi Arabia.
E-mail address: haelabidi@uqu.edu.sa (Haykel Elabidi).

two–body Darwin and orbit–orbit are incorporated. More details of these interactions and how they are incorporated can be found in [12-14], here, we present only a brief description of the theory.

The non–relativistic case is described by the Hamiltonian:

$$H_{nr} = \sum_{i=1}^{N} h_i + \sum_{j>i}^{N+1} \frac{2}{r_{ij}}, \text{ and } h_i = -\nabla_i^2 - \frac{2Z}{r_i}, \quad (1)$$

where N is the number of electrons, Z is the nuclear charge, the energy is expressed in Ry and lengths are given in units of the Bohr radius $a_0 = \hbar^2/me^2 = 0.529$ Å. The problem of N body with $N > 1$ cannot be solved rigorously. The approximate solutions satisfy the variational principle:

$$\delta\{\langle f|H - E|f'\rangle\} = 0. \quad (2)$$

f and f' are the trial functions ($f = C\alpha SL$) where C is a given configuration and α is a degeneracy parameter used when more than one term with the same SL correspond to a specific configuration C. With the Hamiltonian given by equation (1), the total spin **S** and the total angular momentum **L** are separately conserved and so the correspondent quantum numbers S and L are "good" quantum numbers for the system. The approximate functions $|fM_SM_L\rangle$ for the $N-$electrons system are developed in terms of Slater states $|u\rangle$ (defined as the product of the N one–electron functions):

$$|f\rangle = \sum_u |u\rangle\langle u|f\rangle, \text{where} |u\rangle = \prod_{q=1}^{N} |n_q l_q \mu_q m_q\rangle, \quad (3)$$

where $n_q l_q \mu_q m_q$ are the quantum numbers of the q^{th} electron. The system obeys the exclusion principle of Pauli and thus the product in equation (3) has to be antisymmetric. The summation over the states u in (3) includes those states satisfying $M_S = \sum_{q=1}^{N} \mu_q$ and $M_L = \sum_{q=1}^{N} m_q$. The non relativistic part is treated in LS coupling. The relativistic interactions are introduced through the $N-$electrons Breit–Pauli Hamiltonian [18]: $H_{BP} = H_{nr} + H_{rc}$, where H_{nr} is given by (1) and:

$$H_{rc} = \sum_{i=1}^{N} \left\{ \underbrace{f_i(mass)}_{\text{massvariation}} + \underbrace{f_i(d)}_{\text{Darwin}} + \underbrace{f(so)}_{\text{spin-orbit}} \right\} + \sum_{i>j} \left\{ \underbrace{g_{ij}(so + so')}_{\text{spin-other-orbit}} + \underbrace{g_{ij}(ss')}_{\text{spin-spin}} + \underbrace{g_{ij}(css')}_{\text{contact-spin-spin}} + \underbrace{g_{ij}(d)}_{\text{Darwin}} + \underbrace{g_{ij}(oo')}_{\text{orbit-orbit}} \right\}. \quad (4)$$

The first sum describes the one–body terms, and the second one describes two–body terms. The three last terms in the second sum represent the two–body non–fine structure interactions which are ignored in SST [14], but incorporated in AS [13]. The expressions of all the terms in equation (4) are given explicitly in [14]. With the introduction of the relativistic corrections through the Hamiltonian H_{BP}, the operators $\mathbf{L}_z$ and $\mathbf{S}_z$ (projections of **L** and **S**) no longer commute with H_{BR} and consequently, M_L and M_S are not "good" quantum numbers. Consequently, we introduce the total angular momentum $\mathbf{J} = \mathbf{S} + \mathbf{L}$ and its projection $\mathbf{J}_z$, where the corresponding quantum numbers J and M_J (with S and L) are now conserved, and the state in this intermediate coupling will be defined by $|\Delta SLJM_J\rangle$, where Δ is a linear combination of the states $|C\alpha SLJM_J\rangle$.

The radiative data are obtained by evaluating the momentum operator **P** corresponding to the type of the transition between the upper (u) and lower (l) states of the transition:

$$\langle u|\mathbf{P}|l\rangle. \quad (5)$$

Depending on the type of the transition, the operator **P** is the electric momentum $\mathbf{P}^{E\lambda}$ for dipole (λ =1), quadrupole (λ =2) and octopole (λ =3) transitions and magnetic momentum $\mathbf{P}^{M\lambda}$ for dipole (λ =1) and quadrupole (λ =2) transitions. All the radiative quantities can be deduced from the line strength $S(u,l) = S(l,u)$ defined by:

$$S^{E\lambda}(u,l) = \left|\langle u|\mathbf{P}^{E\lambda}|l\rangle\right|^2 \text{ and } S^{M\lambda}(u,l) = \left|\langle u|\mathbf{P}^{M\lambda}|l\rangle\right|^2. \quad (6)$$

For the electric dipole transitions, the absorption oscillator strength (dimensionless) is expressed in terms of the line strength (in atomic unit, 1 a.$u.$ = 6.460×10^{-36} cm ^{2}.esu ^{2}):

$$f_{lu} = \frac{303.75}{g_l \lambda_{ul}} S^{E1}, \quad g_l f_{lu} = -g_u f_{ul} = gf \quad (7)$$

g_u and g_l are the statistical weights of the upper and lower levels and λ_{ul} is the transition wavelength in Å. We give here the expressions of the radiative decay rates (in s $^{-1}$) for each type of transition in terms of the line strength (π is the parity of the system):

• For the electric dipole (E1) transitions ($\Delta J = 0, \pm 1$ and $\Delta\pi \neq 0$):

$$A_{ul}^{E1} = \frac{2.0261\times10^{18}}{g_u \lambda_{ul}^3} S^{E1} \quad (8)$$

• For the electric quadrupole (E2) transitions ($\Delta J = 0, \pm 1, \pm 2$ and $\Delta\pi = 0$):

$$A_{ul}^{E2} = \frac{1.1199\times10^{18}}{g_u \lambda_{ul}^5} S^{E2} \quad (9)$$

• For the electric octopole (E3) transitions ($\Delta J = \pm 2, \pm 3$ and $\Delta\pi \neq 0$):

$$A_{ul}^{E3} = \frac{3.1435\times10^{17}}{g_u \lambda_{ul}^7} S^{E3} \quad (10)$$

• For the magnetic dipole (M1) transitions ($\Delta J = 0, \pm 1, \pm 2$ and $\Delta\pi = 0$):

$$A_{ul}^{M1} = \frac{2.6974\times10^{13}}{g_u \lambda_{ul}^3} S^{M1} \quad (11)$$

• For the magnetic quadrupole (M2) transitions ($\Delta J = 0, \pm 1, \pm 2$ and $\Delta\pi \neq 0$):

$$A_{ul}^{M2} = \frac{1.4910\times10^{13}}{g_u \lambda_{ul}^5} S^{M2} \quad (12)$$

The quantities defined by equations (6−12) are evaluated in the code AS.

2.2. Electron scattering theory

Dimensionless collision strength Ω is related to the cross section σ by the following relationship:

$$\Omega(E) = \frac{k_i^2 g_i}{\pi a_0^2} \sigma(E), \quad (13)$$

where k_i is the incident electron energy in Ry, g_i is the statistical weight of the initial level and a_0 is the Bohr r*adius in cm. Both collision strength and cross section describe the intrinsic probability of collisional excitation and de-excitation in an atomic transition at a particular electron energy, but collision strength is preferred because it is symmetric and dimensionless.

Recently, the Breit–Pauli Distorted Wave (BPDW) approach for electron-impact excitation of atomic ions has been implemented in the AS code [13], which we use it for the scattering problem in the present paper. In AS, the hole system is described by an antisymmetric wavefunction Ψ consisting in a wavefunction ψ for the N-electrons emitter and a scattered free electron wavefunction ϕ:

$$\Psi = \mathcal{A}\psi\phi. \quad (14)$$

Equation (14) does not couple the emitter states and this represents the assumption of the distorted wave approach. The partial collision strengths are evaluated in the code AS using the corresponding transition matrix T [13]:

$$\Omega_{\alpha\beta,\alpha'\beta'} = g_\beta \left|T_{\alpha\beta,\alpha'\beta'}\right|^2 \quad (15)$$

α labels the emitter state and β labels all the other quantum numbers defining the scattering. g_β is the statistical weight of the hole system (scattered electron+emitter), it is equal to $(2J + 1)$ in our case. The transition matrices are evaluated between levels in the coupled representation which are obtained from those in the uncoupled representation through the following relation [19]:

$$|\Gamma_i S_i L_i J_i l K s J\rangle = \sum_{SL} (-1)^{-J_i - 2S_i - J - l - s} [L\ J_i\ K\ S]^{\frac{1}{2}} \begin{Bmatrix} L & l & L_i \\ J_i & S_i & K \end{Bmatrix} \begin{Bmatrix} L & J & S \\ s & S_i & K \end{Bmatrix} |\Gamma_i L_i l L S_i s S J\rangle$$

where capital letters refer to the total system quantum numbers, those with indices refer to the emitter quantum numbers and l and s are for the colliding electron. Terms in braces are the 6–j symbols [20] and $[a, b, \ldots] = (2a + 1)(2b + 1)\ldots$. We note that the distorted wave approximation (DW) is adequate for moderately and highly charged ions and the agreement between the DW and more sophisticated methods (close coupling for example) is good. Collision strengths are calculated at the same set of final scattered energies for all transitions: zero gives all threshold transitions, for example. It is known that collision strengths converge slowly with angular momentum for allowed transitions, consequently, for large l values, a 'top-up' for dipole transitions making use of the sum rule of Burgess and Sheorey [21] is used. For higher multipoles, a geometric series in energy in combination with the degenerate energy limit [22] is used to take into account large l contributions to collision strengths.

As it is mentioned before, in some cases we show a comparison between the results of the AS code and the UCL ones SST/DW/JAJOM. In SST [14], the scaling parameters λ_l depend only on l and the two–body non–fine structure operators of the Breit–Pauli Hamiltonian are omitted. SST supplies also the so called Term Coupling Coefficients (TCC) which will be used in compiling fine structure collision strengths in a next step. The DW code [15]

calculates collision strengths in LS coupling schema, and then fine structure collision strengths for low partial waves l of the incoming electron (in our case l up to 25) are obtained by the JAJOM code [16]. This code uses the reactance matrix elements in LS coupling together with the TCC obtained from the structure calculations to obtain collision strengths in intermediate coupling. For large values of l, the above method becomes cumbersome and inaccurate but the contributions of these values of l to collision strengths cannot be neglected. For $l \geq 26$, we have adopted two different procedures: for allowed transitions, the contribution has been taken into account using the JAJOM-CBe program (Dubau, unpublished results) based upon the Coulomb-Bethe formulation of Burgess and Sheorey [19] and adapted to JAJOM. For forbidden transitions, the contribution has been estimated by the SERIE-GEOM program (Dubau, unpublished results) assuming a geometric series behaviour for high partial wave collision strengths [23,24].

3. Results and Discussions

3.1. Energy levels and lifetimes

We have used in our work 12 configurations: 3s ^{2}**3**p, 3s3p ^{2}, 3s ^{2}3d, 3p ^{3}, 3s3p3d, 3s ^{2}4s, 3s ^{2}4p, 3p ^{2}3d, 3s ^{2}4d, 3s3p4s, 3s3p4p and 3s3p4d yielding to 121 fine structure levels. The scaling parameters ($\boldsymbol{\lambda_{nl}}$) from the code AS used in our calculations are presented in the following Table:

nl	1s	2s	2p	3s	3p	3d	4s	4p	4d
λ_{nl}	2.16164	1.12732	1.04711	1.12692	1.08290	1.09618	1.11797	1.06717	1.08986

We presented in Table 1 our 121 fine structure levels. For the available 60 lowest levels, we compared with the results of Froese Fischer *et al.* [8] and with those from NIST [11]. Calculated lifetimes for the 121 levels and fine structure splitting were also provided. We recalled that the lifetime τ for a level j is defined as follow:

$$\tau_j = \frac{1}{\sum_i A_{ji}} (16)$$

where A_{ji} is the radiative decay rate (Eq. 8) from the level j to all the possible lower levels (here levels corresponding to electric dipole transitions E1).

Our level energies showed a good agreement with the MCHF results [8] and NIST [11] ones. The averaged difference didn't exceed 3 %, except for the levels 35 and 36, and from 39 to 42 (3s3p3d ^{2}P^o, ^{2}D^o and ^{2}F^o), the difference is about 5 %. We will see later that this difference has an influence on the agreement of radiative data. In three cases (marked in **bold** in Table 1), high differences have been found in the term splitting between our results and those from the MCHF formalism [8]. These three cases were recapitulated in Table 2. We noted that for these cases also, our energies and the MCHF ones agree well (about 2 %). We remarked also that the disagreement in the splitting existed also for the results of NIST [11].

Table 1: Our energy levels (E) in cm $^{-1}$ for Ar VI compared to the MCHF [8] and to those from the NIST database [11], and their lifetimes τ. Levels marked by ($*$) are inverted regrading to the MCHF ones. a$E\pm b$ means a$\times 10^{\pm b}$.

i	Conf.	Level	E	Split	MCHF	NIST	τ(s)
1	3s ^{2}3p	^{2}P$^o_{1/2}$	0		0	0	
2	3s ^{2}3p	^{2}P$^o_{3/2}$	2193	2193	2047.39	2207.88	
3	3s3p ^{2}	^{4}P$^o_{1/2}$	98527		98746.57	100157.5	2.49162E−06
4	3s3p ^{2}	^{4}P$^o_{3/2}$	99318	791	99486.49	100957.6	1.06021E−05
5	3s3p ^{2}	^{4}P$^o_{5/2}$	100550	2023	100619.02	102191.6	4.46445E−06
6	3s3p ^{2}	^{2}D$_{3/2}$	132837		131753.79	132462.7	2.68797E−09
7	3s3p ^{2}	^{2}D$_{5/2}$	132941	104	131850.54	132 574.7	2.83518E−09
8	3s3p ^{2}	^{2}S$_{1/2}$	182207		170176.45	169803.9	1.52380E−10
9	3s3p ^{2}	^{2}P$_{1/2}$	186817		184439.40	182182.1	6.92884E−11
10	3s3p ^{2}	^{2}P$_{3/2}$	187971	1154	185742.72	183577.3	6.59349E−11
11	3s ^{2}3d	^{2}D$_{3/2}$	226446		220303.14	218595.9	5.02145E−11
12	3s ^{2}3d	^{2}D$_{5/2}$	226570	124	220425.89	218655.8	5.13475E−11
13	3p ^{3}	^{2}D$^o_{3/2}$	259969		260240.43	260068.7	1.60535E−09
14	3p ^{3}	^{2}D$^o_{5/2}$	260172	203	260438.99	260272.9	1.58868E−09
15	3p ^{3}	^{4}S$^o_{3/2}$	276426		271519.72	270511.8	7.00082E−11
16	3s3p3d	^{4}F$^o_{3/2}$	290227		289823.12	–	2.35284E−07
17	3s3p3d	^{4}F$^o_{5/2}$	290666	439	290245.49	–	1.86730E−07
18	3s3p3d	^{4}F$^o_{7/2}$	291293	1066	290847.72	–	2.10417E−07
19	3s3p3d	^{4}F$^o_{9/2}$	292119	1892	–	–	–
20	3p ^{3}	^{2}P$^o_{3/2}$	302062		294030.80	294086.0	1.81863E−10
21	3p ^{3}	^{2}P$^o_{1/2}$	302227	165	294908.42	294101.3	1.79490E−10
22	3s3p3d	^{4}P$^o_{5/2}$	317702		316397.02	316351.	7.79352E−11
23	3s3p3d	^{4}P$^o_{3/2}$	318264	562	316939.22	316974.	7.67369E−11
24	3s3p3d	^{4}P$^o_{1/2}$	318668	966	317346.50	317459.	7.66836E−11
25	3s3p3d	^{4}D$^o_{1/2}$	322184		319648.31	319273.	4.89429E−11
26	3s3p3d	^{4}D$^o_{3/2}$	322409	225	319881.51	319539.	4.93415E−11
27	3s3p3d	^{4}D$^o_{5/2}$	322676	492	320128.54	319771.	4.95428E−11
28	3s3p3d	^{4}D$^o_{7/2}$	322908	724	320314.56	319905.	4.94792E−11
29	3s3p3d	^{2}D$^o_{5/2}$	340542		329993.40	328960.4	5.56251E−11
30	3s3p3d	^{2}D$^o_{3/2}$	340608	66	330027.48	328992.	5.55703E−11

Table 1: Continued.

i	Conf.	Level	*E*	Split	MCHF	NIST	τ(s)
31	3s ^{2}4s	^{2}S $_{1/2}$	351315		342005.10	342302.	5.13580E−11
32	3s3p3d	^{2}F$^o_{5/2}$	354312		344753.74	344309.8	1.08695E−10
33	3s3p3d	^{2}F$^o_{7/2}$	356046	1734	346387.33	346076.	1.06337E−10
34	3s3p3d	^{2}P$^o_{3/2}$	388109		376940.45	375657.8	4.35879E−11
35	3s3p3d	^{2}P$^o_{1/2}$	388405	296	377374.76	–	4.46216E−11
36	3s3p3d	^{2}F$^o_{7/2}$	398287		378377.68	376421.	4.01109E−11
37	3s3p3d	^{2}F$^o_{5/2}$	398760	473	378802.50	376905.	3.97745E−11
38	3s ^{2}4p	^{2}P$^o_{1/2}$	400653		389461.60	–	1.18727E−10
39	3s ^{2}4p	^{2}P$^o_{3/2}$	401062	409	389633.73	–	1.16972E−10
40	3s3p3d	^{2}D$^o_{3/2}$	418963 *		398713.63	395494.	2.50441E−11
41	3s3p3d	^{2}D$^o_{5/2}$	419532 *	569	399043.44	395807.	2.43203E−11
42	3s3p3d	^{2}P$^o_{1/2}$	419881 *		396100.64	–	2.89757E−11
43	3s3p3d	^{2}P$^o_{3/2}$	420223 *	342	396568.11	–	2.84833E−11
44	3p ^{2}3d	^{4}F $_{3/2}$	448677		–	–	1.43142E−10
45	3p ^{2}3d	^{4}F $_{5/2}$	449117	440	–	–	1.42676E−10
46	3p ^{2}3d	^{4}F $_{7/2}$	449743	1066	–	–	1.42015E−10
47	3p ^{2}3d	^{4}F $_{9/2}$	450558	1881	–	–	1.41173E−10
48	3s3p4s	^{4}P$^o_{1/2}$	455089		453718.27	454096.	7.63457E−11
49	3s3p4s	^{4}P$^o_{3/2}$	455807	718	454441.10	454874.	7.64552E−11
50	3s3p4s	^{4}P$^o_{5/2}$	457074	1985	455734.06	456280.	7.67432E−11
51	3p ^{2}3d	^{4}D $_{1/2}$	457611			–	1.27696E−10
52	3p ^{2}3d	^{4}D $_{3/2}$	457777	166		–	1.27602E−10
53	3p ^{2}3d	^{4}D $_{5/2}$	457888	277		–	1.44789E−10
54	3p ^{2}3d	^{4}D $_{7/2}$	458058	447		–	1.45251E−10
55	3p ^{2}3d	^{2}F $_{5/2}$	459061			–	2.62343E−10
56	3p ^{2}3d	^{2}F $_{7/2}$	460472	1411		–	2.57006E−10
57	3p ^{2}3d	^{2}P $_{3/2}$	462127			–	7.41930E−11
58	3p ^{2}3d	^{2}P $_{1/2}$	463691	1564		–	7.31090E−11
59	3s ^{2}4d	^{2}D $_{3/2}$	465362			454751.	2.36279E−10
60	3s ^{2}4d	^{2}D $_{5/2}$	465420	58		454807.	2.30475E−10

Table 1: Continued.

i	Conf.	Level	*E*	τ(s)	*i*	Conf.	Level	*E*	τ(s)
61	3s3p4s	^{2}P$^o_{1/2}$	472094	6.06111E−11	92	3p ^{2}3d	^{2}D $_{5/2}$	560675	2.70723E−11
62	3s3p4s	^{2}P$^o_{3/2}$	473486	5.94949E−11	93	3p ^{2}3d	^{2}D $_{3/2}$	561606	2.70336E−11
63	3p ^{2}3d	^{2}G $_{7/2}$	483923	4.49121E−10	94	3s3p4d	^{4}D$^o_{3/2}$	568023	1.80540E−10
64	3p ^{2}3d	^{2}G $_{9/2}$	484086	4.53471E−10	95	3s3p4d	^{4}D$^o_{1/2}$	568045	1.71875E−10
65	3p ^{2}3d	^{4}P $_{5/2}$	489801	2.82277E−11	96	3s3p4d	^{4}D$^o_{5/2}$	568135	1.82025E−10
66	3p ^{2}3d	^{4}P $_{3/2}$	490368	2.80070E−11	97	3s3p4d	^{4}D$^o_{7/2}$	568531	1.78977E−10
67	3p ^{2}3d	^{4}P $_{1/2}$	490671	2.79000E−11	98	3s3p4d	^{4}F$^o_{3/2}$	569174	3.86712E−10
68	3p ^{2}3d	^{2}D $_{5/2}$	499460	3.82183E−11	99	3s3p4d	^{4}F$^o_{5/2}$	569727	3.89187E−10
69	3p ^{2}3d	^{2}D $_{3/2}$	499571	3.80270E−11	100	3s3p4d	^{2}D$^o_{3/2}$	570181	3.89371E−10
70	3s3p4p	^{4}D $_{1/2}$	500380	2.41899E−10	101	3s3p4d	^{2}D$^o_{5/2}$	570442	3.75059E−10
71	3s3p4p	^{4}D $_{3/2}$	500920	2.44565E−10	102	3s3p4d	^{4}F$^o_{7/2}$	570567	3.90887E−10
72	3s3p4p	^{4}D $_{5/2}$	501794	2.47776E−10	103	3s3p4d	^{4}F$^o_{9/2}$	571148	4.61991E−10
73	3s3p4p	^{4}D $_{7/2}$	502954	2.46570E−10	104	3s3p4d	^{4}P$^o_{5/2}$	574207	2.36460E−10
74	3s3p4p	^{2}P $_{1/2}$	503633	1.42575E−10	105	3s3p4d	^{4}P$^o_{3/2}$	574719	2.40067E−10
75	3s3p4p	^{2}P $_{3/2}$	503960	1.42132E−10	106	3s3p4d	^{4}P$^o_{1/2}$	575032	2.42982E−10
76	3s3p4p	^{4}S $_{3/2}$	508141	2.41812E−10	107	3s3p4d	^{2}F$^o_{5/2}$	577336	2.26096E−10
77	3s3p4p	^{4}P $_{1/2}$	509018	1.84588E−10	108	3s3p4p	^{2}P $_{1/2}$	578471	5.40903E−11
78	3s3p4p	^{4}P $_{3/2}$	509736	1.92658E−10	109	3s3p4d	^{2}F$^o_{7/2}$	578473	2.24880E−10
79	3s3p4p	^{4}P $_{5/2}$	510261	1.85721E−10	110	3s3p4p	^{2}P $_{3/2}$	578956	5.39334E−11
80	3p ^{2}3d	^{2}D $_{3/2}$	512284	7.30063E−11	111	3s3p4p	^{2}D $_{3/2}$	580817	5.22153E−11
81	3s3p4p	^{2}D $_{5/2}$	513909	7.34621E−11	112	3s3p4p	^{2}D $_{5/2}$	581163	5.23804E−11
82	3p ^{2}3d	^{2}S $_{1/2}$	518616	4.70268E−11	113	3s3p4d	^{2}P$^o_{3/2}$	581968	1.85910E−10
83	3s3p4p	^{2}D $_{3/2}$	522641	1.66337E−10	114	3s3p4d	^{2}P$^o_{1/2}$	582723	1.82666E−10
84	3p ^{2}3d	^{2}D $_{5/2}$	523977	1.63683E−10	115	3s3p4p	^{2}S $_{1/2}$	591134	5.69581E−11
85	3s3p4p	^{2}S $_{1/2}$	531376	1.03863E−10	116	3s3p4d	^{2}D$^o_{3/2}$	638746	5.47023E−11
86	3s3p4s	^{2}P$^o_{1/2}$	532709	3.47490E−11	117	3s3p4d	^{2}D$^o_{5/2}$	638822	5.44126E−11
87	3s3p4s	^{2}P$^o_{3/2}$	532853	3.50560E−11	118	3s3p4d	^{2}F$^o_{5/2}$	642340	1.02040E−10
88	3p ^{2}3d	^{2}F $_{5/2}$	541730	2.59138E−11	119	3s3p4d	^{2}F$^o_{7/2}$	642351	1.01992E−10
89	3p ^{2}3d	^{2}F $_{7/2}$	541825	2.58749E−11	120	3s3p4d	^{2}P$^o_{1/2}$	649049	4.80934E−11
90	3p ^{2}3d	^{2}P $_{1/2}$	545089	3.54412E−11	121	3s3p4d	^{2}P$^o_{3/2}$	649139	4.77992E−11
91	3p ^{2}3d	^{2}P $_{3/2}$	545837	3.54137E−11					

Table 2: Splitting (Split) between our levels. MCHF stands for the results of [8] and NIST for those of [11].

Index	Conf.	Level	E	MCHF	NIST	Split	Split (MCHF)	Split (NIST)
20	$3p^3$	$^2P^o_{3/2}$	302062	294030.80	294086.0			
21	$3p^3$	$^2P^o_{1/2}$	302227	294908.42	294101.3	165	877.62	15.3
29	3s3p3d	$^2D^o_{5/2}$	340542	329993.40	328960.4			
30	3s3p3d	$^2D^o_{3/2}$	340608	330027.48	328992.	66	34.08	31.6
34	3s3p3d	$^2P^o_{3/2}$	388109	376940.45	375657.8			
35	3s3p3d	$^2P^o_{1/2}$	388405	377374.76	–	296	434.31	–

3.2. Radiative data

We presented in Table 3 our line strengths (S), oscillator strengths in absorption (f_{ik}) and radiative decay rates (A_{ki}) for electric dipole (E1) transitions from the lowest 12 levels to the lowest 43 ones (belonging to the first seven configurations $3s^2 3p$, $3s3p^2$, $3s^2 3d$, $3p^3$, 3s3p3d, $3s^2 4s$ and $3s^2 4p$). Our results for electric dipole transitions were compared to the MCHF ones [8], since they were the only provided in this reference. We excluded from our tables transitions that were not provided in [8] or those for which the radiative decay rates are less than 10^4 s^{-1}. Differences between the two results were ranging from 2 % to 50 % with an averaged difference of about 25 %. Almost all the transitions presenting a huge difference involved levels from 35 to 42 ($3s3p3d$ $^2P^o$, $^2D^o$ and $^2F^o$). As we mentioned in the precedent subsection, the energies of these levels presented the most important disagreement ($\simeq$ 5 %) between our values and those of [8]. This could be one of the origins of the difference in the radiative data.

Radiative atomic data for forbidden transitions (E2, M1) were presented in Table 4 and those for forbidden transitions (E3, M2) were presented in Table 5. To the best of our knowledge, there were no radiative data for Ar VI forbidden transitions. These parameters are the first to be published, and may be of high interest in plasma modelling. Transitions for which the type was designed as E2/M1 was a mix of electric quadrupole and magnetic dipole transitions. The presented values of line strengths (S) and radiative decay rates (A_{ki}) correspond to the most probable process: $A_{ki} = \max(A_{ki}^{E2}, A_{ki}^{M1})$. In the database NIST [11], only the results of one forbidden transition $3s^2 3p\ ^2P_{1/2} - 3s^2 3p\ ^2P^o_{3/2}$ $(1-2)$ has been found. The results of this transition were presented in the Table below, and the agreement between them and our values is good.

$i-k$	S	S^{NIST}	A_{ki}	A_{ki}^{NIST}
$1-2$	1.333E+00	1.3E+00	9.484E−02	9.7E−02

Table 3: Our line strengths (S), oscillator strengths in absorption (f_{ik}) and radiative decay rates (A_{ki}) for electric dipole E1 transitions compared to MCHF ones [8]. a$E\pm b$ means a$\times 10^{\pm b}$. i and k label the levels in Table 1.

Trans.	S		f_{ik}		A_{ki} (s^{-1})	
$i-k$	Present	MCHF	Present	MCHF	Present	MCHF
1 − 3	2.603E−04	2.966E−04	4.000E−05	4.449E−05	2.522E+05	2.894E+05
1 − 4	8.752E−06	1.211E−05	1.320E−06	1.829E−06	4.343E+03	6.038E+03
1 − 6	2.763E−01	3.560E−01	5.575E−02	7.124E−02	3.281E+08	4.125E+08
1 − 8	7.839E−01	4.536E−01	2.169E−01	1.172E−01	4.804E+09	2.265E+09
1 − 9	1.093E+00	1.448E+00	3.103E−01	4.055E−01	7.223E+09	9.201E+09
1 − 10	7.879E−01	7.941E−01	2.249E−01	2.240E−01	2.650E+09	2.578E+09
1 − 11	2.807E+00	2.800E+00	9.653E−01	9.367E−01	1.651E+10	1.516E+10
1 − 31	1.463E−01	1.606E−01	7.808E−02	8.343E−02	6.428E+09	6.510E+09
2 − 3	1.647E−04	2.225E−04	3.895E−05	1.634E−05	1.491E+05	2.039E+05
2 − 4	1.939E−04	1.796E−04	1.430E−05	1.329E−05	8.998E+04	8.414E+04
2 − 5	6.971E−04	7.448E−04	5.207E−05	5.575E−05	2.240E+05	2.409E+05
2 − 6	3.891E−02	5.313E−02	3.860E−03	5.233E−03	4.395E+07	5.872E+07
2 − 7	4.673E−01	6.051E−01	4.640E−02	5.965E−02	3.527E+08	4.469E+08
2 − 8	2.975E−01	5.597E−01	4.068E−02	7.146E−02	1.758E+09	2.695E+09
2 − 9	1.131E+00	8.896E−01	1.585E−01	1.232E−01	7.210E+09	5.468E+09
2 − 10	3.854E+00	3.897E+00	5.437E−01	5.436E−01	1.252E+10	1.224E+10
2 − 11	5.964E−01	5.943E−01	1.016E−01	9.849E−02	3.407E+09	3.130E+09
2 − 12	5.105E+00	5.096E+00	8.699E−01	8.450E−01	1.948E+10	1.792E+10
3 − 13	5.932E−05	–	1.455E−05	–	1.264E+05	–
3 − 15	8.534E−01	8.532E−01	2.306E−01	2.239E−01	2.434E+09	2.229E+09
3 − 16	2.355E−04	2.327E−04	6.856E−05	6.752E−05	8.403E+05	8.222E+05
3 − 20	1.447E−03	–	4.472E−04	–	6.179E+06	–
3 − 21	7.996E−06	–	2.474E−06	–	6.847E+04	–
3 − 23	1.402E+00	1.338E+00	4.679E−01	4.434E−01	7.536E+09	7.041E+09
3 − 24	3.283E−01	3.465E−01	1.098E−01	1.150E−01	3.549E+09	3.666E+09
3 − 25	1.385E+00	1.254E+00	4.704E−01	4.208E−01	1.569E+10	1.370E+10
3 − 26	1.117E+00	9.434E−01	3.799E−01	3.169E−01	6.351E+09	5.168E+09
4 − 15	1.705E+00	1.705E+00	2.293E−01	2.227E−01	4.798E+09	4.396E+09
4 − 16	3.193E−04	3.031E−04	4.629E−05	4.381E−05	1.125E+06	1.059E+06
4 − 17	1.255E−03	1.216E−03	1.823E−04	1.761E−04	2.969E+06	2.850E+06
4 − 20	2.894E−03	–	4.455E−04	–	1.222E+07	–
4 − 21	9.949E−05	–	1.533E−05	–	8.420E+05	–
4 − 22	1.748E+00	1.699E+00	2.899E−01	2.798E−01	6.148E+09	5.855E+09
4 − 23	1.179E−01	4.937E−02	1.960E−02	8.153E−03	6.268E+08	2.571E+08
4 − 24	8.877E−01	6.924E−01	1.479E−01	1.145E−01	9.491E+09	7.253E+09
4 − 25	4.224E−01	4.462E−01	7.149E−02	7.460E−02	4.737E+09	4.824E+09
4 − 26	2.139E+00	2.054E+00	3.623E−01	3.437E−01	1.203E+10	1.114E+10
4 − 27	3.151E+00	2.823E+00	5.345E−01	4.730E−01	1.186E+10	1.024E+10

Table 3: Continued.

Trans.	S		f_{ik}		A_{ki} (s $^{-1}$)	
$i-k$	Present	MCHF	Present	MCHF	Present	MCHF
5 − 13	1.313E−04	–	1.060E−05	–	2.695E+05	–
5 − 14	4.644E−04	–	3.753E−05	–	6.378E+05	–
5 − 15	2.559E+00	2.557E+00	2.278E−01	2.212E−01	7.051E+09	6.464E+09
5 − 16	2.855E−05	3.195E−05	2.742E−06	3.061E−06	9.870E+04	1.096E+05
5 − 17	5.581E−04	5.498E−04	5.371E−05	5.278E−05	1.295E+06	1.266E+06
5 − 18	2.620E−03	2.562E−03	2.530E−04	2.467E−04	4.605E+06	4.467E+06
5 − 20	1.249E−03	–	1.274E−04	–	5.176E+06	–
5 − 22	1.932E+00	–	2.124E−01	–	6.681E+09	–
5 − 23	9.307E−01	–	1.026E−01	–	4.865E+09	–
5 − 26	3.405E−01	3.712E−01	3.824E−02	4.120E−02	1.883E+09	1.982E+09
5 − 27	2.247E+00	2.249E+00	2.527E−01	2.499E−01	8.318E+09	8.032E+09
5 − 28	7.256E+00	6.868E+00	8.168E−01	7.639E−01	2.020E+10	1.844E+10
6 − 13	4.400E−01	5.371E−01	4.248E−02	5.240E−02	4.579E+08	5.770E+08
6 − 14	5.464E−02	7.125E−02	5.283E−03	6.963E−03	3.809E+07	5.128E+07
6 − 15	6.793E−05	–	7.408E−06	–	1.019E+05	–
6 − 16	9.437E−04	1.120E−03	1.128E−04	1.344E−04	1.864E+06	2.240E+06
6 − 20	1.885E−01	1.771E−01	2.422E−02	2.182E−02	4.627E+08	3.834E+08
6 − 21	1.006E+00	9.206E−01	1.294E−01	1.141E−01	4.954E+09	4.051E+09
6 − 29	4.325E−01	4.032E−01	6.822E−02	6.070E−02	1.309E+09	1.061E+09
6 − 30	3.501E+00	3.265E+00	5.523E−01	4.916E−01	1.590E+10	1.289E+10
6 − 32	2.248E+00	1.897E+00	3.781E−01	3.068E−01	8.247E+09	6.190E+09
6 − 34	4.429E−03	6.093E−03	8.586E−04	1.134E−03	3.732E+07	4.549E+07
6 − 35	2.448E−02	3.519E−02	4.750E−03	6.563E−03	4.139E+08	5.282E+08
6 − 37	1.910E+00	1.897E+00	3.857E−01	3.068E−01	1.213E+10	6.190E+09
6 − 38	1.025E−01	9.226E−02	2.084E−02	1.806E−02	1.994E+09	1.600E+09
6 − 39	2.165E−02	1.973E−02	4.410E−03	3.863E−03	2.116E+08	1.714E+08
6 − 40	4.053E−03	–	8.807E−04	–	4.809E+07	–
7 − 13	7.465E-02	9.116E−02	4.801E−03	5.925E−03	7.751E+07	9.773E+07
7 − 14	7.309E−01	8.895E−01	4.708E−02	5.791E−02	5.083E+08	6.387E+08
7 − 15	2.838E−04	–	2.062E−05	–	4.247E+05	–
7 − 16	1.571E−04	2.873E−04	1.251E−05	2.298E−05	3.097E+05	5.738E+05
7 − 17	7.995E−04	1.013E−03	6.384E−05	8.122E−05	1.059E+06	1.359E+06
7 − 18	1.090E−04	1.407E−04	8.741E−06	1.132E− 05	1.097E+05	1.432E+05
7 − 20	1.789E+00	1.624E+00	1.532E−01	1.334E−01	4.384E+09	3.510E+09
7 − 22	1.235E−03	–	1.155E−04	–	2.630E+06	–
7 − 23	5.866E−04	–	5.504E−05	–	1.891E+06	–
7 − 26	4.776E−04	–	4.581E−05	–	1.645E+06	–
7 − 28	4.345E−03	–	4.179E−04	–	7.544E+06	–
7 − 29	5.393E+00	5.029E+00	5.668E−01	5.044E−01	1.629E+10	1.321E+10
7 − 30	3.679E−01	3.439E−01	3.867E−02	3.450E−02	1.669E+09	1.356E+09

Table 3: Continued.

Trans.	S		f_{ik}		A_{ki} (s $^{-1}$)	
$i-k$	Present	MCHF	Present	MCHF	Present	MCHF
7 − 32	2.020E−01	1.730E−01	2.264E−02	1.865E−02	7.401E+08	5.639E+08
7 − 33	3.261E+00	2.721E+00	3.684E−01	2.955E−01	9.173E+09	6.805E+09
7 − 34	3.665E−02	5.253E−02	4.735E−03	6.518E−03	3.085E+08	3.917E+08
7 − 36	2.721E+00	2.721E+00	3.656E−01	2.955E−01	1.288E+10	6.805E+09
7 − 37	1.294E−01	1.730E−01	1.742E−02	1.865E−02	8.210E+08	5.639E+08
7 − 39	1.950E−01	1.754E−01	2.647E−02	2.289E−02	1.904E+09	1.522E+09
7 − 40	2.165E−04	–	3.135E−05	–	2.566E+06	–
7 − 41	3.561E−03	–	5.166E−04	–	2.830E+07	–
7 − 43	1.195E−04	–	1.737E−05	–	1.435E+06	–
8 − 13	3.172E−02	5.700E−03	3.747E−03	7.797E−04	7.556E+06	2.109E+06
8 − 20	2.109E−01	2.942E−01	3.840E−02	5.534E−02	1.840E+08	2.831E+08
8 − 21	2.133E−02	1.026E−01	3.888E−03	1.944E−02	3.736E+07	2.017E+08
8 − 34	3.995E+00	3.236E+00	1.249E+00	1.016E+00	1.766E+10	1.449E+10
8 − 35	1.380E+00	1.437E+00	4.321E−01	4.523E−01	1.225E+10	1.295E+10
8 − 38	1.399E−01	1.579E−02	4.643E−02	5.258E−03	1.478E+09	1.687E+08
8 − 39	4.486E−01	3.713E−02	1.491E−01	1.238E−02	2.382E+09	1.988E+08
8 − 40	1.025E−01	1.823E−02	3.686E−02	6.327E−03	6.892E+08	1.102E+08
8 − 42	3.475E−01	2.890E−01	1.254E−01	9.915E−02	4.726E+09	3.376E+09
8 − 43	2.250E−01	4.538E−01	8.133E−02	1.560E−01	1.537E+09	2.667E+09
9 − 13	3.387E−01	4.665E−01	3.763E−02	5.371E−02	6.715E+07	1.029E+08
9 − 16	1.216E−05	2.806E−05	1.910E−06	4.492E−06	6.813E+03	1.664E+04
9 − 20	3.869E−02	1.169E−01	6.772E−03	1.945E−02	3.000E+07	7.793E+07
9 − 21	2.753E−01	3.616E−01	4.825E−02	6.068E−02	4.287E+08	4.939E+08
9 − 30	1.463E−01	1.787E−01	3.416E−02	3.951E−02	2.695E+08	2.793E+08
9 − 34	6.492E−03	–	1.985E−03	–	2.682E+07	–
9 − 35	7.887E−01	4.705E−01	2.415E−01	1.379E−01	6.546E+09	3.423E+09
9 − 38	2.013E−01	4.945E−01	6.537E−02	1.540E−01	1.994E+09	4.318E+09
9 − 39	1.051E−02	3.357E−01	3.420E−03	1.046E−01	5.236E+07	1.469E+09
9 − 40	4.612E+00	4.028E+00	1.626E+00	1.311E+00	2.923E+10	2.007E+10
9 − 42	7.632E−01	4.631E−01	2.701E−01	1.489E−01	9.788E+09	4.449E+09
9 − 43	1.835E−03	4.839E−01	6.506E−04	1.559E−01	1.182E+07	2.340E+09
10 − 13	6.180E−02	7.363E−02	3.379E−03	4.166E−03	1.168E+07	1.542E+07
10 − 14	6.431E−01	8.104E−01	3.526E−02	4.597E−02	8.173E+07	1.140E+08
10 − 15	1.545E−03	–	1.038E−04	–	5.417E+05	–
10 − 20	5.490E−01	8.244E−01	4.757E−02	6.779E−02	4.130E+08	5.303E+08
10 − 21	9.868E−02	1.537E−01	8.562E−03	1.274E−02	1.491E+08	2.026E+08
10 − 29	2.586E−01	2.922E−01	2.996E−02	3.201E−02	3.101E+08	2.962E+08
10 − 30	3.864E−02	4.242E−02	4.478E−03	4.647E−03	6.959E+07	6.454E+07
10 − 34	7.649E−01	9.668E−01	1.162E−01	1.548E−01	3.106E+09	4.589E+09

Table 3: Continued.

Trans.	S		f_{ik}		A_{ki} (s $^{-1}$)	
$i-k$	Present	MCHF	Present	MCHF	Present	MCHF
10 − 35	1.392E−01	2.657E−01	2.119E−02	4.245E−02	1.135E+09	2.506E+09
10 − 37	9.221E−04	–	1.476E−04	–	2.916E+06	–
10 − 38	6.045E−02	2.547E−01	9.763E−03	3.940E−02	5.891E+08	2.182E+09
10 − 39	2.619E−01	1.129E+00	4.237E−02	1.748E−01	1.283E+09	4.846E+09
10 − 40	6.570E−02	1.210E+00	1.152E−02	1.957E−01	4.102E+08	5.920E+09
10 − 41	7.702E+00	7.981E+00	1.354E+00	1.293E+00	3.229E+10	2.615E+10
10 − 42	5.183E−01	2.657E−01	9.129E−02	4.245E−02	6.550E+09	2.506E+09
10 − 43	3.243E+00	9.668E−01	5.719E−01	1.548E−01	2.058E+10	4.589E+09
11 − 1	2.843E−02	5.225E−02	7.236E−04	1.585E−03	5.424E+05	1.686E+06
11 − 14	2.770E−03	–	7.093E−05	–	3.588E+04	–
11 − 16	2.838E−05	8.551E−05	1.375E−06	4.515E−06	3.730E+03	1.455E+04
11 − 17	3.214E−04	3.760E−04	1.567E−05	1.997E−05	2.875E+04	4.345E+04
11 − 30	5.691E−02	–	4.934E−03	–	4.289E+07	–
11 − 32	2.707E−01	–	2.628E−02	–	1.911E+08	–
11 − 34	1.056E−01	5.443E−02	1.296E−02	7.286E−03	2.260E+08	1.510E+08
11 − 35	4.736E−01	6.892E−01	5.825E−02	9.201E−02	2.038E+09	3.793E+09
11 − 37	6.606E+00	4.281E+00	8.645E−01	5.153E−01	1.141E+10	5.756E+09
11 − 38	3.703E−01	1.423E+00	4.898E−02	1.827E−01	1.983E+09	6.976E+09
11 − 39	7.093E−02	2.462E−01	9.406E−03	3.166E−02	1.913E+08	6.056E+08
11 − 40	1.258E+00	2.387E+00	1.840E−01	3.234E−01	4.548E+09	6.867E+09
11 − 41	2.004E−01	2.104E−01	2.938E−02	2.855E−02	4.871E+08	4.057E+08
11 − 42	1.832E+00	6.892E−01	2.691E−01	9.201E−02	1.343E+10	3.793E+09
11 − 43	1.335E+00	5.443E−02	1.965E−01	7.286E−03	4.922E+09	1.510E+08
12 − 13	3.410E-03	–	5.766E-05	–	6.436E+04	–
12 − 14	4.413E−02	8.176E−02	7.508E−04	1.656E−03	5.654E+05	1.769E+06
12 − 18	5.494E−04	5.910E−04	1.800E−05	2.107E−05	3.773E+04	5.227E+04
12 − 20	6.310E−03	–	2.411E−04	–	1.375E+06	–
12 − 22	3.935E−04	–	1.815E−05	–	1.006E+05	–
12 − 23	6.650E−05	–	3.087E−06	–	2.597E+04	–
12 − 26	2.150E−04	–	1.043E−05	–	9.588E+04	–
12 − 28	3.100E−04	–	1.512E−05	–	7.020E+04	–
12 − 29	8.624E−02	1.853E−01	4.976E−03	1.028E−02	4.311E+07	8.230E+07
12 − 30	4.785E−03	–	2.763E−04	–	3.595E+06	–
12 − 32	2.819E−02	5.099E−02	1.823E−03	3.209E−03	1.984E+07	3.309E+07
12 − 33	4.012E−01	7.623E−01	2.630E−02	4.861E−02	2.205E+08	3.858E+08
12 − 34	7.263E−01	2.557E−01	5.940E−02	2.026E−02	1.551E+09	4.966E+08
12 − 36	9.393E+00	6.064E+00	8.166E−01	4.849E−01	1.205E+10	6.052E+09
12 − 37	4.477E−01	2.829E−01	3.903E−02	2.268E−02	7.719E+08	3.795E+08
12 − 39	7.890E−01	2.903E+00	6.969E−02	2.487E−01	2.123E+09	7.123E+09
12 − 40	1.386E+00	–	1.350E−01	–	4.999E+09	–

Table 4: Our line strengths S(a.u) and radiative decay rates A_{ki} (s $^{-1}$) for electric quadrupole (E2) and magnetic dipole (M1) transitions $i-j$ where $1 \leq i \leq 31$ and j up to the level 43.

$i-k$	S^{E2}	S^{M1}	A_{ki}^{E2}	A_{ki}^{M1}	$i-k$	S^{E2}	S^{M1}	A_{ki}^{E2}	A_{ki}^{M1}
1 − 2	2.585E+00	1.333E+00	3.673E−06	9.484E−02	**2 − 13**	1.492E+00	2.518E−06	4.754E+04	2.909E−01
1 − 13	1.668E+00	8.392E−07	5.546E+04	9.943E−02	**2 − 14**	3.654E+00	1.314E−06	7.793E+04	1.014E−01
1 − 14	1.077E+00	0.000E+00	2.397E+04	0.000E+00	**2 − 15**	2.561E−03	4.652E−06	1.112E+02	6.470E−01
1 − 15	1.528E−03	1.017E−06	6.906E+01	1.449E−01	**2 − 16**	1.508E−05	8.888E−09	8.371E-01	1.432E−03
1 − 16	5.109E−05	2.319E−08	2.945E+00	3.822E−03	**2 − 17**	6.119E−05	9.015E−09	2.282E+00	9.728E−04
1 − 17	5.141E−07	0.000E+00	1.991E−02	0.000E+00	**2 − 18**	3.353E−05	0.000E+00	9.479E-01	0.000E+00
1 − 20	1.032E+00	1.408E−06	7.270E+04	2.617E−01	**2 − 20**	1.240E+00	3.093E−10	8.416E+04	5.624E−05
1 − 22	3.125E−05	0.000E+00	1.888E+00	0.000E+00	**2 − 21**	1.120E+00	1.632E−06	1.525E+05	5.946E−01
1 − 23	2.209E−06	5.349E−09	2.020E−01	1.163E−03	**2 − 22**	1.037E−04	4.216E−07	6.049E+00	5.953E−02
1 − 24	0.000E+00	8.745E−08	0.000E+00	3.817E−02	**2 − 23**	1.814E−05	1.470E−07	1.602E+00	3.130E−02
1 − 25	0.000E+00	2.212E−07	0.000E+00	9.976E−02	**2 − 24**	2.962E−06	6.675E−08	5.266E-01	2.853E−02
1 − 26	2.298E−06	5.227E−07	2.241E−01	1.181E−01	**2 − 25**	2.831E−05	8.577E−08	5.319E+00	3.790E−02
1 − 27	2.705E−07	0.000E+00	1.766E−02	0.000E+00	**2 − 26**	2.645E−05	1.100E−07	2.493E+00	2.436E−02
1 − 29	2.050E−01	0.000E+00	1.752E+04	0.000E+00	**2 − 27**	6.689E−06	6.500E−07	4.221E-01	9.619E−02
1 − 30	2.663E−01	4.821E−07	3.418E+04	1.285E−01	**2 − 28**	3.541E−06	0.000E+00	1.682E-01	0.000E+00
1 − 32	6.143E+00	0.000E+00	6.403E+05	0.000E+00	**2 − 29**	5.122E−01	3.389E−07	4.240E+04	5.901E−02
1 − 34	1.906E+00	7.710E−07	4.699E+05	3.040E−01	**2 − 30**	2.137E−01	9.542E−07	2.655E+04	2.494E−01
1 − 35	0.000E+00	7.191E−10	0.000E+00	5.683E−04	**2 − 32**	1.787E+00	5.450E−10	1.805E+05	1.070E−04
1 − 37	1.829E−02	0.000E+00	3.441E+03	0.000E+00	**2 − 33**	1.057E+01	0.000E+00	8.210E+05	0.000E+00
1 − 38	0.000E+00	1.741E−08	1.512E−02	0.000E+00	**2 − 34**	1.767E+00	1.511E−08	4.234E+05	5.857E−03
1 − 39	3.246E−01	8.278E−06	9.430E+04	3.601E+00	**2 − 35**	1.869E+00	1.225E−06	8.994E+05	9.515E−01
1 − 40	1.609E+00	1.825E−07	5.815E+05	9.048E−02	**2 − 36**	3.799E−02	0.000E+00	5.185E+03	0.000E+00
1 − 41	7.106E−01	0.000E+00	1.724E+05	0.000E+00	**2 − 37**	9.852E−03	7.096E−09	1.804E+03	1.990E−03
1 − 42	0.000E+00	1.649E−10	0.000E+00	1.646E−04	**2 − 38**	3.564−01	1.019E−05	2.005E+05	8.692E+00
1 − 43	1.145E−01	9.979E−07	4.201E+04	4.993E−01	**2 − 39**	3.993E−01	2.587E−07	1.129E+05	1.107E−01

Table 4: Continued.

$i-k$	S^{E2}	S^{M1}	A_{ki}^{E2}	A_{ki}^{M1}	$i-k$	S^{E2}	S^{M1}	A_{ki}^{E2}	A_{ki}^{M1}
3 − 4	3.370E−01	3.330E+00	2.927E−09	1.113E−02	**5 − 12**	5.525E−04	9.534E−05	3.278E−01	8.578E−01
3 − 5	3.026E+00	0.000E+00	1.914−06	0.000E+00	**5 − 31**	4.835E−04	0.000E+00	2.685E+01	0.000E+00
3 − 6	8.486E−04	4.399E−04	1.211E−01	1.198E−01	**6 − 7**	2.367E+00	2.398E+00	5.472E−13	1.226E−05
3 − 7	2.573E−05	0.000E+00	2.318E−05	0.000E+00	**6 − 8**	3.026E+00	2.169E−05	4.969E+01	3.521E−02
3 − 8	0.000E+00	3.644E−04	0.000E+00	2.800E+00	**6 − 9**	5.455E−01	3.400E−04	1.400E+01	7.212E−01
3 − 9	0.000E+00	3.019E−05	0.000E+00	2.869E−01	**6 − 10**	1.072E−01	1.121E−03	1.529E+00	1.266E+00
3 − 10	9.137E−05	4.323E−05	1.464E−02	2.086E−01	**6 − 11**	3.836E−02	1.137E−07	7.720E+00	6.291E−04
3 − 11	6.926E−04	6.106E−06	6.642E−01	8.619E−02	**6 − 12**	1.604E−02	9.463E−07	2.167E+00	3.504E−03
3 − 12	8.085E−04	0.000E+00	5.194E−01	0.000E+00	**6 − 31**	6.160E−01	3.677E−11	1.717E+04	5.172E−06
3 − 31	0.000E+00	1.442E−08	0.000E+00	3.143E−03	**7 − 8**	5.154E+00	0.000E+00	8.376E+01	0.000E+00
4 − 5	4.224E+00	3.597E+00	2.235E−07	3.022E−02	**7 − 9**	1.648E−01	0.000E+00	4.189E+00	0.000E+00
4 − 6	1.882E−04	1.742E−03	2.229E−04	4.424E−01	**7 − 10**	1.505E−01	6.573E−04	2.127E+00	7.387E−01
4 − 7	5.811E−03	1.524E−03	4.661E−03	2.604E−01	**7 − 11**	1.529E−02	1.361E−06	3.061E+00	7.503E−03
4 − 8	3.750E−05	1.341E−03	8.217E−03	1.030E+01	**7 − 12**	6.369E−02	5.043E−10	8.554E+00	1.861E−06
4 − 9	3.021E−04	8.854E−05	8.677E−02	8.000E−01	**7 − 31**	9.296E−01	0.000E+00	2.585E+04	0.000E+00
4 − 10	2.020E−04	1.006E−04	3.098E−02	4.727−01	**8 − 9**	0.000E+00	1.777E−01	0.000E+00	2.347E−01
4 − 11	1.618E−05	2.447E−05	1.540E−02	3.390E−01	**8 − 10**	1.331E−01	9.586E−02	2.371E−05	1.238E−01
4 − 12	8.630E−05	1.736E−05	5.375E−02	1.608E−01	**8 − 11**	1.467E+00	8.497E−06	6.960E+00	4.961E−03
4 − 31	4.616E−05	6.703E−08	2.627E+00	1.447E−02	**8 − 12**	2.287E+00	0.000E+00	7.336E+00	0.000E+00
5 − 6	5.072E−03	6.231E−04	4.983E−03	1.414E−01	**8 − 31**	0.000E+00	2.853E−08	1.861E−03	0.000E+00
5 − 7	2.110E−02	7.652E−03	1.404E−02	1.169E+00	**9 − 10**	1.928E+00	1.237E+00	1.104E−07	1.281E−02
5 − 8	1.191E−03	0.000E+00	2.422E−01	0.000E+00	**9 − 11**	1.596E−01	1.068E−04	4.368E−01	4.481E−02
5 − 9	9.077E−05	0.000E+00	2.428E−02	0.000E+00	**9 − 12**	1.434E−01	0.000E+00	2.658E−01	0.000E+00
5 − 10	3.448E−07	1.237E−04	4.929E−05	5.573E−01	**9 − 31**	0.000E+00	4.087E−07	0.000E+00	2.454E−02
5 − 11	1.377E−04	6.689E−06	1.220E−01	9.001E−02	**10 − 11**	3.105E−04	3.778E-04	7.330−04	1.451E−01

Table 5: Same as in Table 4 but for electric octopole (E3) and magnetic quadrupole (M2) transitions.

$i-k$	S^{E3}	S^{M2}	A_{ki}^{E3}	A_{ki}^{M2}	$i-k$	S^{E3}	S^{M2}	A_{ki}^{E3}	A_{ki}^{M2}
1 −5	1.677E−03	1.764E+01	9.130E−08	4.505E−02	9−41	5.010E+00	7.689E+00	9.704E−02	1.304E+00
1 −7	2.699E+00	4.108E+01	1.038E−03	4.238E−01	10−18	5.505E−04	1.801E−03	2.720E−08	3.953E−06
3 −12	7.918E+00	2.368E+00	1.272E−01	3.513E−01	10−19	7.422E−04	0.000E+00	3.102E−08	0.000E+00
3 −14	2.896E−05	4.409E+00	4.376E−08	1.209E−01	10−28	1.034E−07	2.378E+01	3.312E−11	1.982E−01
8 −14	1.618E−01	1.606E+00	1.485E−06	1.150E−03	10−33	1.516E+01	1.087E+01	2.258E−02	2.716E−01
8 −17	1.128E−03	1.862E−04	1.043E−07	6.943E−07	10−36	3.227E+00	2.576E+00	2.308E−02	1.976E−01
8 −18	1.903E−03	0.000E+00	1.375E−07	0.000E+00	11−18	4.198E−05	5.797E+00	7.957E−11	1.239E−03
8 −22	1.479E−04	2.090E+01	6.498E−08	2.371E−01	11−19	4.657E−05	0.000E+00	7.715E−11	0.000E+00
8 −27	2.052E−04	4.079E−04	1.161E−07	5.543E−06	11−28	1.742E−04	5.291E+00	5.321E−09	8.235E−03
8 −28	5.409E−04	0.000E+00	2.321E−07	0.000E+00	11−33	2.466E−01	4.702E+01	5.952E−05	3.204E−01
8 −29	1.570E−02	1.922E+01	2.053E−05	4.752E−01	11−36	5.125E−01	6.286E+00	8.913E−04	1.755E−01
8 −32	5.248E+00	3.179E−01	1.230E−02	1.193E−02	12−19	3.245E−04	1.739E+01	5.306E−10	3.138E−03
8 −33	1.544E+00	0.000E+00	2.911E−03	0.000E+00	12−21	2.222E−01	3.940E−01	4.957E−06	7.280E−04
8 −36	1.179E+01	0.000E+00	1.019E−01	0.000E+00	12−24	1.794E−04	8.882E−01	1.585E−08	4.387E−03
8 −37	5.841E+00	1.115E−01	6.836E−02	1.320E−02	12−25	5.327E−04	2.155E+00	6.119E−06	1.284E−02
8 −41	3.266E−01	7.346E−01	7.258E−03	1.374E−01	12−35	1.264E+01	6.741E+00	5.776E−02	5.579E−01
9 −14	2.032E+00	2.564E+00	1.217E−05	1.353E−03	12−38	2.113E+01	8.320E+00	1.610E−01	9.916E−01
9 −17	1.575E−05	1.330E−02	1.075E−09	3.992E−05	12−42	1.188E−01	5.000E−01	1.884E−03	1.006E−01
9 −18	1.146E−04	0.000E+00	6.121E−09	0.000E+00	14−31	3.212E−07	5.163E−03	2.639E−11	2.421E−05
9 −22	1.378E−03	6.108E+00	4.752E−07	5.830E−02	17−31	3.054E−05	4.402E−06	1.449E−10	2.693E−09
9 −27	2.244E−04	8.276E+00	1.005E−07	9.519E−02	18−31	5.687E−05	0.000E+00	2.510E−10	0.000E+00
9 −28	3.417E−05	0.000E+00	1.161E−08	0.000E+00	22−31	1.073E−07	2.982E−02	8.183E−15	9.539E−07
9 −29	2.893E−01	1.973E+01	3.075E−04	4.209E−01	27−31	1.038E−05	7.715E−04	2.580E−13	1.108E−08
9 −32	4.332E+00	5.336E+00	8.397E−03	1.748E−01	28−31	6.932E−05	0.000E+00	1.627E−12	0.000E+00
9 −33	7.135E+00	0.000E+00	1.115E−02	0.000E+00	29−31	3.271E−05	4.397E−02	8.664E−16	4.757E−09
9 −36	1.467E−02	0.000E+00	1.090E−04	0.000E+00	31−36	5.087E−01	0.000E+00	1.009E−07	0.000E+00
9 −37	3.634E+00	1.559E+00	3.658E−02	1.656E−01	31−41	3.574E−02	1.552E−02	1.288E−10	5.697E−06

3.3. Collision strengths

We presented in Table 6 our collision strengths calculated using the code AS [13]. We selected the transitions from the ten lowest levels to the 21 other ones: Ω_{ik} with $i = 1-5$ and $k = 2-21$. Levels are belonging to the first five configurations 3s ^{2}3p, 3s3p ^{2}, 3s ^{2}3d, 3p ^{3} and four levels (^{4}F $^{o}_{3/2-9/2}$) from the configuration 3s3p3d. Collision strengths are provided at six electron energies 10, 50, 100, 200, 400 and 800 Ry. For illustration, we present in Figure 1 collision strengths for 4 transitions as a function of electron energy calculated using the AS code and using the UCL codes SST/DW/JAJOM. We remark that for M1 and E2 transitions $1-2$ (3s ^{2}3p ^{2}P $^{o}_{1/2}$ −3s ^{2}3p ^{2}P $^{o}_{3/2}$) and $2-30$ (3s ^{2}3p ^{2}P $^{o}_{3/2}$ −3s3p3d ^{2}D $^{o}_{3/2}$) displayed in panels (a) and (b) of Figure1, the collision strengths from AS converge well to the infinite energy Born limits. This is not true for the electric dipole transitions $1-6$ (3s ^{2}3p ^{2}P $^{o}_{1/2}$ −3s3p ^{2} ^{2}D $_{3/2}$) and $1-11$ (3s ^{2}3p ^{2}P $^{o}_{1/2}$ −3s ^{2}3d ^{2}D $_{3/2}$) displayed in panels c and d of Figure 1, where we found that the corresponding collision strengths do not converge to the Born limit as the UCL results. We remark also that the collision strengths from AS of some transitions have the same behaviour as those from UCL but they are not in good agreement with them such as the transition 3s ^{2}3p ^{2}P $^{o}_{3/2}$ −3s3p3d ^{2}D $^{o}_{3/2}$ (2−30). There are no other collisional results provided as collision strengths Ω to compare with.

Table 6: Excitation collision strengths (Ω_{ik}) for transitions from the lowest ◦ levels to the other 21 ones (levels from configurations 3s ^{2}3p, 3s3p ^{2}, 3s ^{2}3d, 3p ^{3}, and some from 3s3p3d). BORN refers to the infinite energy Born limits. aE$\pm b$ means $a \times 10^{\pm b}$.

$i-k$	10 Ry	50 Ry	100 Ry	200 Ry	400 Ry	800 Ry	BORN
1 −2	6.080E−01	5.859E−01	5.827E−01	5.668E−01	4.853E−01	3.298E−01	5.63E−01
1 −3	1.575E−02	2.673E−03	2.238E−03	2.446E−03	2.718E−03	3.037E−03	3.47E−04
1 −4	2.094E−02	1.301E−03	2.127E−04	9.799E−05	9.536E−05	1.032E−04	1.17E−05
1 −5	1.294E−02	7.891E−04	1.131E−04	3.675E−05	2.605E−05	1.717E−05	2.94E−05
1 −6	1.130E+00	1.692E+00	2.054E+00	2.377E+00	2.677E+00	3.012E+00	3.68E−01
1 −7	6.397E−02	4.056E−02	4.205E−02	4.278E−02	3.743E−02	2.603E−02	4.62E−02
1 −8	2.615E+00	3.957E+00	4.990E+00	5.931E+00	6.819E+00	7.822E+00	1.05E+00
1 −9	3.626E+00	5.486E+00	6.929E+00	8.243E+00	9.473E+00	1.085E+01	1.46E+00
1 −10	2.597E+00	3.919E+00	4.953E+00	5.899E+00	6.788E+00	7.793E+00	1.05E+00
1 −11	7.916E+00	1.210E+01	1.571E+01	1.911E+01	2.240E+01	2.616E+01	3.74E+00
1 −12	7.883E−02	9.918E−02	1.074E−01	1.092E−01	9.440E−02	6.510E−02	1.19E−01
1 −13	2.340E−01	3.251E−01	3.494E−01	3.508E−01	3.019E−01	2.061E−01	3.58E−01
1 −14	1.516E−01	2.103E−01	2.259E−01	2.264E−01	1.943E−01	1.328E−01	2.31E−01
1 −15	3.374E−04	3.204E−04	3.312E−04	3.307E−04	2.862E−04	1.957E−04	3.36E−04
1 −16	1.236E−02	8.545E−04	1.563E−04	3.401E−05	1.297E−05	7.121E−06	1.16E−05
1 −17	1.430E−02	9.782E−04	1.680E−04	2.628E−05	3.604E−06	4.441E−07	1.39E−07
1 −18	1.094E−02	7.507E−04	1.290E−04	2.029E−05	2.827E−06	3.456E−07	8.40E−08
1 −19	9.892E−05	1.355E−05	1.800E−06	1.932E−07	7.954E−08	1.588E−08	0.00E+00
1 −20	1.398E−01	2.013E−01	2.181E−01	2.198E−01	1.898E−01	1.296E−01	2.24E−01
1 −21	6.022E−04	5.193E−04	5.174E−04	5.121E−04	4.983E−04	4.145E−04	5.07E−04

Table 6: Continued.

$i-k$	10 Ry	50 Ry	100 Ry	200 Ry	400 Ry	800 Ry	BORN
2 −3	9.593E−03	1.669E−03	1.414E−03	1.548E−03	1.722E−03	1.927E−03	2.20E−04
2 −4	2.676E−02	2.902E−03	1.791E−03	1.855E−03	2.046E−03	2.276E−03	2.59E−04
2 −5	6.036E−02	8.281E−03	6.163E−03	6.610E−03	7.319E−03	8.154E−03	9.29E−04
2 −6	2.409E−01	2.901E−01	3.413E−01	3.836E−01	4.154E−01	4.486E−01	5.19E−02
2 −7	1.976E+00	2.909E+00	3.520E+00	4.062E+00	4.563E+00	5.122E+00	6.23E−01
2 −8	9.920E−01	1.496E+00	1.886E+00	2.243E+00	2.583E+00	2.970E+00	3.97E−01
2 −9	3.755E+00	5.680E+00	7.169E+00	8.525E+00	9.801E+00	1.124E+01	1.51E+00
2 −10	1.276E+01	1.932E+01	2.440E+01	2.903E+01	3.337E+01	3.827E+01	5.14E+00
2 −11	1.797E+00	2.710E+00	3.483E+00	4.195E+00	4.864E+00	5.629E+00	7.95E−01
2 −21	1.522E−01	2.183E−01	2.367E−01	2.389E−01	2.068E−01	1.413E−01	2.44E−01
3 −4	1.421E−01	8.135E−02	7.733E−02	7.458E−02	6.388E−02	4.346E−02	7.39E−02
3 −5	6.764E−01	6.889E−01	6.877E−01	6.695E−01	5.741E−01	3.911E−01	6.64E−01
3 −6	1.770E−02	1.388E−03	4.289E−04	2.346E−04	1.751E−04	1.158E−04	1.93E−04
3 −7	1.116E−02	7.111E−04	1.407E−04	3.072E−05	9.323E−06	4.192E−06	5.66E−06
3 −8	2.170E−03	2.652E−04	5.758E−05	9.419E−06	3.718E−06	2.462E−06	2.96E−06
3 −9	3.942E−04	9.442E−05	2.282E−05	2.972E−06	5.865E−07	1.537E−07	9.07E−09
3 −10	3.167E−03	2.370E−04	6.171E−05	2.624E−05	1.708E−05	1.085E−05	1.90E−05
3 −11	2.914E−03	3.364E−04	1.801E−04	1.453E−04	1.184E−04	7.954E−05	1.41E−04
3 −12	2.165E−03	2.864E−04	1.846E−04	1.605E−04	1.316E−04	8.855E−05	1.60E−04
3 −13	3.029E−02	1.944E−03	5.684E−04	4.793E−04	5.361E−04	6.109E−04	7.91E−05
3 −14	6.388E−03	3.680E−04	5.265E−05	5.968E−06	8.717E−07	2.770E−07	4.06E−07
3 −15	2.923E+00	4.406E+00	5.529E+00	6.549E+00	7.504E+00	8.580E+00	1.14E+00
3 −16	5.474E−03	1.427E−03	1.473E−03	1.709E−03	1.979E−03	2.296E−03	3.14E−04
3 −17	4.694E−02	6.604E−02	7.172E−02	7.328E−02	6.390E−02	4.433E−02	7.94E−02
3 −18	8.060E−02	1.202E−01	1.309E−01	1.337E−01	1.165E−01	8.074E−02	1.45E−01
3 −19	3.554E−03	2.144E−04	3.747E−05	4.987E−06	4.657E−07	2.994E−08	0.00E+00
3 −20	8.016E−03	7.082E−03	8.774E−03	1.049E−02	1.213E−02	1.399E−02	1.93E−03
3 −21	5.634E−03	3.830E−04	9.136E−05	6.450E−05	7.054E−05	7.921E−05	1.07E−05

Table 6: Continued.

$i-k$	10 Ry	50 Ry	100 Ry	200 Ry	400 Ry	800 Ry	BORN
4 −5	1.017E+00	9.680E−01	9.621E−01	9.356E−01	8.012E−01	5.454E−01	9.27E−01
4 −6	2.751E−02	1.874E−03	3.912E−04	9.733E−05	3.922E−05	2.108E−05	3.53E−05
4 −7	3.171E−02	3.300E−03	1.704E−03	1.363E−03	1.124E−03	7.596E−04	1.29E−03
4 −8	4.027E−03	4.902E−04	1.090E−04	2.143E−05	1.024E−05	6.271E−06	9.41E−06
4−9	2.017E−03	2.913E−04	1.145E−04	7.044E−05	5.526E−05	3.685E−05	6.43E−05
4 −10	5.740E−03	5.029E−04	1.366E−04	5.731E−05	3.820E−05	2.456E−05	4.26E−05
4 −11	4.644E−03	3.276E−04	6.661E−05	1.443E−05	4.721E−06	2.194E−06	3.34E−06
4 −12	5.140E−03	3.692E−04	8.952E−05	3.416E−05	2.137E−05	1.347E−05	2.16E−05
4 −13	4.115E−02	2.432E−03	4.940E−04	3.098E−04	3.288E−04	3.641E−04	4.58E−05
4 −14	3.108E−02	2.021E−03	5.986E−04	4.877E−04	5.430E−04	6.216E−04	8.07E−05
4−15	5.857E+00	8.834E+00	1.108E+01	1.312E+01	1.503E+01	1.717E+01	2.27E+00
4 −16	8.655E−02	1.258E−01	1.328E−01	1.246E−01	9.695E−02	6.167E−02	4.26E−04
4 −17	5.472E−02	7.134E−02	7.596E−02	7.272E−02	5.936E−02	4.253E−02	1.67E−03
4 −18	1.125E−02	7.513E−04	1.557E−04	5.016E−05	3.262E−05	2.175E−05	4.00E−05
4 −19	1.204E−01	1.753E−01	1.907E−01	1.945E−01	1.694E−01	1.171E−01	2.11E−01
4 −20	1.975E−02	1.455E−02	1.777E−02	2.118E−02	2.443E−02	2.809E−02	3.86E−03
4 −21	9.193E−03	1.013E−03	6.614E−04	7.231E−04	8.333E−04	9.619E−04	1.33E−04
5 −6	2.561E−02	2.668E−03	5.457E−03	1.139E−03	9.322E−04	6.281E−04	1.08E−03
5 −7	6.804E−02	8.860E−03	4.049E−04	4.661E−03	3.862E−03	2.609E−03	4.51E−03
5 −8	5.546E−03	8.829E−04	1.115E−04	2.923E−04	2.442E−04	1.661E−04	2.76E−04
5 −9	6.256E−03	4.819E−04	1.584E−04	3.597E−05	2.065E−05	1.273E−05	2.06E−05
5 −10	6.567E−03	7.303E−04	9.358E−05	2.344E−05	4.362E−06	1.036E−06	1.18E−07
5 −11	4.501E−03	3.268E−04	2.722E−04	4.833E−05	3.545E−05	2.322E−05	3.71E−05
5 −12	1.050E−02	8.553E−04	1.067E−03	1.546E−04	1.173E−04	7.696E−05	1.29E−04
5 −13	1.431E−02	1.567E−03	3.868E−03	1.122E−03	1.243E−03	1.387E−03	1.75E−04
5 −14	9.394E−02	7.703E−03	1.663E+01	3.913E−03	4.364E−03	4.889E−03	6.19E−04
5 −15	8.767E+00	1.326E+01	3.125E−02	1.969E+01	2.255E+01	2.579E+01	3.41E+00
5 −16	2.418E−02	2.988E−02	1.089E−01	2.914E−02	2.245E−02	1.406E−02	3.80E−05
5 −17	7.520E−02	1.033E−01	2.133E−01	1.020E−01	7.952E−02	5.181E−02	7.44E−04
5 −18	1.439E−01	2.010E−01	2.334E−01	2.017E−01	1.611E−01	1.116E−01	3.49E−03
5 −19	1.597E−01	2.152E−01	7.917E−03	2.377E−01	2.064E−01	1.431E−01	2.58E−01
5 −20	3.055E−02	7.707E−03	6.277E−05	9.242E−03	1.062E−02	1.217E−02	1.66E−03
5 −21	5.797E−03	3.891E−04	1.104E+01	1.956E−05	1.429E−05	9.644E−06	1.74E−05

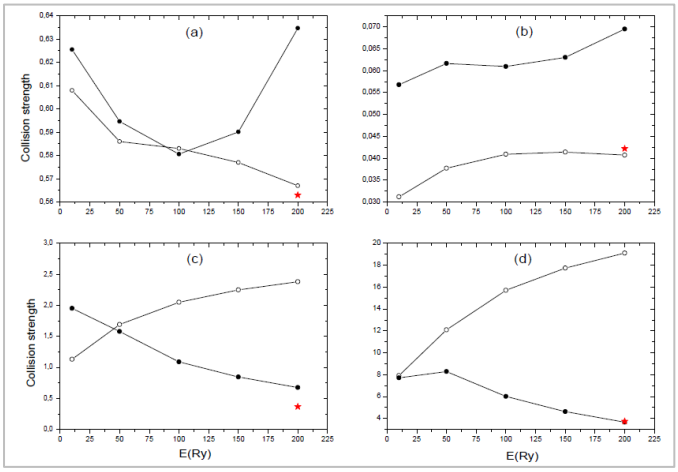

Figure 1: Collision strength as a function of electron energy for the 4 selected transitions: $3s\,^2 3p\;\; ^2P^o_{1/2} - 3s\,^2 3p\;\; ^2P^o_{3/2}$ (a: 1−2), $3s\,^2 3p\;\; ^2P^o_{1/2} - 3s3p3d\;\; ^2D_{3/2}$ (b: 2 − 30), $3s\,^2 3p\;\; ^2P^o_{1/2} - 3s3p\,^2\;\; ^2D_{3/2}$ (c: 1 − 6) and $3s\,^2 3p\;\; ^2P^o_{1/2} - 3s\,^2 3d\;\; ^2D_{3/2}$ (d: 1 − 11). ◦: AS, •: UCL, ⋆: infinite energy Born limits.

It is known that collision strengths are determined by summing over the total angular momentum J, consequently, it is important to ensure that we have included all the values of J that contribute to the collision strengths; i.e. check that as J increases its contribution for Ω decreases and approximately tends to zero. We examine here this convergence problem with the angular momentum J. For illustration, we present in Figure 2 the contributions of each angular momentum J to the partial collision strengths Ω_J at different electron energies for some transitions. As it is known for electric dipole transitions, collision strengths do not converge easily with J, and we have to take into account the contributions of higher partial waves especially at high energies. This case is illustrated in panels (c) and (d) of Figure 2 respectively for the $3s\,^2 3p\;\; ^2P^o_{1/2} - 3s3p\,^2\;\; ^2D_{3/2}$ transition $(1-6)$ and the $3s3p3d\;\; ^2D^o_{3/2} - 3p\,^2 3d\;\; ^4D_{3/2}$ one $(30-52)$, where collision strengths start to converge for high J (90−100) at electron energy $E = 150$ Ry. The two forbidden transitions $3s\,^2 3p\;\; ^2P^o_{1/2} - 3s\,^2 3p\;\; ^2P^o_{3/2}$ $(1-2)$ and $3s\,^2 3p\;\; ^2P^o_{3/2} - 3s3p3d\;\; ^4F^o_{5/2}$ $(2-17)$ (panels a and b of Figure 2) converge easily (for $J = 35-45$) as it is expected even at high energies. A first conclusion can be drawn from the above discussions is that all the necessary angular momenta that contribute to the collision strengths are well introduced, and so our collisional calculations are sufficiently complete.

3.4. Effective collision strengths

In a hot plasma, electrons have a wide range of velocities (energies), then collision strength Ω are averaged over a given velocities distribution to provide effective collision strength Υ. Assuming a thermodynamic equilibrium state, a Maxwellian distribution is chosen. Hence, effective collision strengths Υ are obtained by convolving the collision strength Ω with the Maxwellian electron energy distribution as follows:

$$\Upsilon_{if}(T_e) = \int_0^\infty \Omega_{if}(E) e^{-E_f/kT_e} \mathrm{d}(E_f/kT_e), \qquad (17)$$

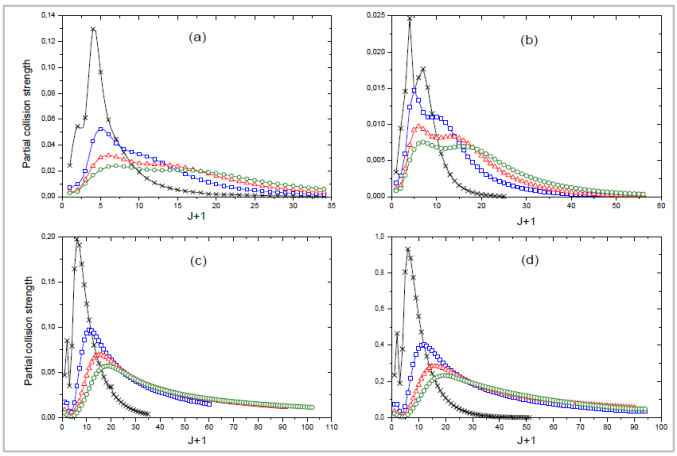

Figure 2: Partial collision strength as a function of the total angular momentum J for several electron energies for the 4 selected transitions: $3s\,^2 3p\;\; ^2P^o_{1/2} - 3s\,^2 3p\;\; ^2P^o_{3/2}$ (a: $1-2$), $3s\,^2 3p\;\; ^2P^o_{3/2} - 3p\,^3\;\; ^2P^o_{1/2}$ (b: $2-17$), $3s\,^2 3p\;\; ^2P^o_{1/2} - 3s3p\,^2\;\; ^2D_{3/2}$ (c: $1-6$) and $3s3p3d\;\; ^2D^o_{3/2} - 3p\,^2 3d\;\; ^4D_{3/2}$ (d: $30-52$) at energies 10 Ry (×), 50 Ry (•), 100 Ry (△) and 150 Ry (◦).

where k is the Boltzman constant, T_e is the electron temperature in K and E_f is the incident electron energy with respect to the final (upper) level. These quantities are dimensionless and are involved in astrophysical and solar applications through the excitation $q(i,f)$ and de-excitation $q(f,i)$ rate coefficients defined as:

$$q(i,f) = \frac{8.629\times10^{-6}}{g_i T_e^{1/2}} \Upsilon(T_e) e^{-\Delta E_{if}/kT_e} \ (\mathrm{cm^3 s^{-1}}) \quad (18)$$

and $$q(f,i) = \frac{8.629\times10^{-6}}{g_f T_e^{1/2}} \Upsilon(T_e) \ (\mathrm{cm^3 s^{-1}}) \quad (19)$$

where g_i and g_f are the statistical weights of the initial (i) and the final (f) levels, respectively, and $\Delta E_{if} = E_f - E_i$ is the corresponding transition energy. The integration in Equation 6 should be carried out using energy-dependent collision strengths from threshold to infinity. The collision strengths at higher energies are particularly important for the dipole allowed transitions, where they grow as $\ln(E)$. In the case of the electric quadrupole or magnetic dipole transitions, the collision strengths are approximately constant, whereas for intercombination transitions they rapidly decrease as $1/E^2$ in the asymptotic region[22].

Our effective collision strengths $\Upsilon_{ik}(T_e)$ are calculated with the code ADASEXJ[1] using the collision strengths Ω from the code AUTOSTRUCTURE. We present in Table 7 $\Upsilon_{ik}(T_e)$ with $i = 1-6$ and $k = 2-21$ over a wide temperature range from 7.2×10^3 K up to 3.6×10^5 K suitable for astrophysical and plasma applications. We compare with the results of [2] obtained by the Breit-Pauli R-matrix method (BPRM)[2]. On the light of these comparison, there are several points that have to be stressed:

• Firstly, we remark that almost all transitions involving the levels from 16 to 21 ($3s3p3d\ ^4F^o_{3/2-9/2}$ and $3p^3\ ^2P^o_{1/2-3/2}$) present effective collision strengths that are not in good agreement with our results. We remark also that levels $16-21$ have not the same order in our calculations as in the calculations of [2], and the disagreement can be due to the inversion of these levels.

• Secondly, Effective collision strengths of electric dipole transitions agree well with the results of [2]. This point is illustrated in Figure 3 (panel c) displaying effective collision strengths of the $1-8$, $1-9$, $1-11$ and $4-15$ allowed transitions. For the forbidden transitions (E2 and M1), the agreement is less than that of the allowed transitions. Figs. 2 (panels a and b) show our results and those of the [2] for four forbidden transitions ($1-17$, $2-20$, $3-6$ and $6-8$).

• Thirdly, we remark that the agreement is as good as the transition is more probable (strong transition). Table 7 shows the fact that the ratio AS/BPRM is varying from 0.16 for the E2 transition $1-17$ with a radiative decay rate $A(1-17) = 1.991\times10^{-2}$ to 0.95 for the E2/M1 transition $2-20$ with $A(2-20) = 8.416\times10^{+4}$. This is also true for allowed transitions where the agreement increases with the strength of the transition: the ratio AS/BPRM increases from 0.29 for the transition $1-4$ with $A(1-4) = 4.343\times10^{+3}$ to 0.99 for the transition $1-11$ with $A(1-11) = 1.651\times10^{+10}$. There are some exceptions that escape this conclusion.

• Finally, we note that for forbidden transitions, the agreement is better for high temperatures (Figure 3, panels a and b), but for electric dipole transitions, the agreement is better for low temperatures (Figure 3, panel c). This can be explained by the fact that for allowed transitions, the contribution of high energies (temperatures) to collision strengths is important, in contrast to intercombination transitions where collision strengths vary rapidly in the asymptotic region (low temperature). We illustrate this remark in the Table 8.

Table 7: Effective collision strengths Υ_{ik} (Present) for transitions from the lowest 6 levels to the other 21 ones compared to BPRM results [2]. $a \pm b$ means $a \times 10^{\pm b}$.

T_e(K)	7.20+03		3.60+04		1.80+05		7.20+05		3.60+05	
$i-k$	Present	BPRM	Present	BPRM	Present	BPRM	Present	BPRM	Present	BPRM
1 −2	8.86−01	6.33+00	8.72−01	6.42+00	8.15−01	4.73+00	7.18−01	2.26+00	6.28−01	3.39+00
1 −3	4.94−02	2.95−01	4.85−02	2.39−01	4.42−02	1.55−01	3.32−02	7.25−02	1.54−02	2.50−02
1 −4	6.99−02	3.77−01	6.86−02	4.07−01	6.24−02	2.64−01	4.63−02	1.21−01	2.03−02	4.55−02
1 −5	4.34−02	5.76−01	4.26−02	5.39−01	3.87−02	3.23−01	2.87−02	1.34−01	1.25−02	4.46−02
1 −6	7.96−01	1.72+00	8.03−01	1.62+00	8.38−01	1.34+00	9.66−01	1.14+00	1.30+00	1.37+00
1 −7	1.65−01	1.53+00	1.62−01	1.23+00	1.48−01	7.13−01	1.14−01	3.17−01	6.75−02	1.24−01
1 −8	1.66+00	1.57+00	1.68+00	1.52+00	1.79+00	1.52+00	2.16+00	1.79+00	3.02+00	2.67+00
1 −9	2.28+00	2.77+00	2.31+00	2.63+00	2.47+00	2.77+00	3.00+00	3.46+00	4.19+00	5.21+00
1 −10	1.67+00	1.94+00	1.69+00	1.85+00	1.80+00	1.89+00	2.17+00	2.25+00	3.01+00	3.30+00
1 −11	4.71+00	4.37+00	4.84+00	4.72+00	5.42+00	5.25+00	6.71+00	6.78+00	9.33+00	1.06+01
1 −12	1.40−01	5.29−01	1.38−01	5.61−01	1.31−01	4.35−01	1.10−01	2.51−01	9.08−02	1.51−01
1 −13	1.97−01	2.99−01	2.00−01	2.77−01	2.15−01	2.45−01	2.31−01	2.56−01	2.61−01	3.06−01
1 −14	1.30−01	2.98−01	1.32−01	2.65−01	1.41−01	1.99−01	1.50−01	1.81−01	1.69−01	2.03−01
1 −15	1.03−03	2.64−02	1.01−03	3.63−02	8.89−04	2.25−02	6.49−04	9.08−03	4.07−04	3.57−03
1 −16	4.36−02	1.35−01	4.27−02	1.06−01	3.85−02	7.25−02	2.80−02	4.08−02	1.21−02	1.56−02
1 −17	5.04−02	1.90−01	4.94−02	1.42−01	4.46−02	9.30−02	3.24−02	5.03−02	1.40−02	1.87−02
1 −18	3.87−02	1.60−01	3.79−02	1.23−01	3.42−02	7.75−02	2.48−02	4.08−02	1.07−02	1.48−02
1 −19	6.62−04	8.78−02	6.38−04	5.61−02	5.30−04	2.76−02	3.34−04	9.97−03	1.30−04	2.31−03
1 −20	1.13−01	1.94−01	1.15−01	1.83−01	1.24−01	1.57−01	1.35−01	1.58−01	1.55−01	1.89−01
1 −21	1.13−03	5.86−02	1.11−03	5.58−02	1.03−03	3.37−02	8.45−04	1.82−02	6.18−04	1.25−02
2 −3	3.01−02	4.70−01	2.95−02	3.77−01	2.69−02	2.23−01	2.02−02	9.12−02	9.42−03	2.66−02
2 −4	8.70−02	7.28−01	8.54−02	7.43−01	7.77−02	4.69−01	5.80−02	2.05−01	2.60−02	7.66−02
2 −5	1.93−01	1.23+00	1.90−01	1.19+00	1.73−01	7.64−01	1.29−01	3.48−01	5.89−02	1.32−01
2 −6	3.22−01	1.91+00	3.19−01	1.64+00	3.06−01	1.04+00	2.81−01	5.53−01	2.69−01	3.57−01
2 −7	1.50+00	3.94+00	1.51+00	3.62+00	1.56+00	2.86+00	1.75+00	2.23+00	2.27+00	2.47+00
2 −8	6.49−01	1.45+00	6.56−01	1.42+00	6.93−01	1.22+00	8.29−01	1.18+00	1.15+00	1.58+00
2 −9	2.40+00	2.81+00	2.43+00	2.39+00	2.59+00	2.41+00	3.12+00	2.91+00	4.34+00	4.36+00
2 −10	8.00+00	7.93+00	8.11+00	7.97+00	8.68+00	8.58+00	1.05+01	1.07+01	1.47+01	1.62+01
2 −11	1.22+00	1.61+00	1.24+00	1.69+00	1.35+00	1.65+00	1.59+00	1.75+00	2.11+00	2.44+00
2 −12	8.69+00	8.44+00	8.92+00	9.10+00	9.99+00	9.95+00	1.23+01	1.26+01	1.70+01	1.95+01
2 −13	1.80−01	4.06−01	1.83−01	3.62−01	1.95−01	2.77−01	2.08−01	2.54−01	2.34−01	2.85−01
2 −14	4.36−01	7.40−01	4.43−01	6.94−01	4.74−01	5.83−01	5.08−01	5.85−01	5.72−01	6.83−01
2 −15	1.82−03	5.14−02	1.77−03	6.98−02	1.56−03	4.35−02	1.13−03	1.76−02	7.01−04	7.11−03
2 −16	1.21−02	1.36−01	1.19−02	9.07−02	1.07−02	5.36−02	7.73−03	2.36−02	3.33−03	7.12−03
2 −17	3.31−02	2.73−01	3.25−02	1.82−01	2.92−02	1.09−01	2.12−02	5.07−02	9.13−03	1.63−02
2 −18	7.28−02	2.90−01	7.13−02	2.25−01	6.43−02	1.47−01	4.66−02	7.77−02	2.01−02	2.85−02
2 −19	1.38−01	3.77−01	1.35−01	3.11−01	1.22−01	2.19−01	8.86−02	1.27−01	3.83−02	4.81−02

[1] http://amdpp.phys.strath.ac.uk/autos/ver/misc/

[2] Data of effective collision strengths have been taken from the website http://open.adas.ac.uk

Table 7: Continued.

T_e(K)	7.20+03		3.60+04		1.80+05		7.20+05		3.60+05	
$i-k$	Present	BPRM	Present	BPRM	Present	BPRM	Present	BPRM	Present	BPRM
3 −4	4.43−01	1.81+00	4.30−01	2.86+00	3.75−0	6.58+00	2.71−01	7.76+00	1.53−01	5.01+00
3 −5	8.03−01	2.46+00	7.96−01	2.80+00	7.66−01	4.07+00	7.21−01	4.74+00	6.92−01	4.02+00
3 −6	1.01−01	4.84−01	9.77−02	4.78−01	8.22−02	3.85−01	5.34−02	2.90−01	2.10−02	2.55−01
3 −7	6.05−02	4.72−01	5.85−02	4.47−01	4.94−02	3.52−01	3.24−02	2.38−01	1.28−02	1.82−01
3−8	1.89−02	1.53−01	1.82−02	1.60−01	1.50−02	1.37−01	9.15−03	1.04−01	3.32−03	1.04−01
3−9	3.14−03	1.22−01	3.01−03	1.58−01	2.43−03	1.87−01	1.48−03	1.07+00	5.67−04	1.66+00
3 −10	1.66−02	1.23−01	1.60−02	2.18−01	1.37−02	2.46−01	9.04−03	6.77−01	3.61−03	9.55−01
3 −11	1.50−02	2.45−01	1.45−02	2.66−01	1.25−02	1.78−01	8.28−03	1.23−01	3.36−03	1.04−01
3 −12	1.02−02	1.91−01	9.92−03	2.35−01	8.55−03	1.65−01	5.78−03	9.82−02	2.41−03	7.47−02
3 −13	1.11−01	3.26−01	1.09−01	3.11−01	9.93−02	1.88−01	7.22−02	1.00−01	3.07−02	3.88−02
3 −14	2.74−02	2.78−01	2.68−02	2.54−01	2.36−02	1.27−01	1.65−02	5.09−02	6.78−03	1.52−02
3 −15	1.91+00	1.94+00	1.93+00	2.07+00	2.04+00	2.11+00	2.44+00	2.51+00	3.37+00	3.65+00
3 −16	2.47−02	4.72−01	2.41−02	2.55−01	2.11−02	1.36−01	1.45−02	5.97−02	6.36−03	1.81−02
3 −17	6.34−02	5.83−01	6.28−02	3.64−01	6.03−02	2.01−01	5.47−02	1.13−01	5.40−02	7.75−02
3 −18	8.94−02	6.07−01	8.91−02	4.02−01	8.79−02	2.26−01	8.49−02	1.45−01	9.27−02	1.23−01
3 −19	1.69−02	3.17−01	1.64−02	1.82−01	1.43−02	8.41−02	9.78−03	3.52−02	3.93−03	9.89−03
3−20	1.63−02	1.85−01	1.61−02	1.37−01	1.51−02	6.30−02	1.24−02	2.87−02	8.90−03	1.43−02
3 −21	2.02−02	1.13−01	1.99−02	8.99−02	1.82−02	4.71−02	1.34−02	2.37−02	5.70−03	8.97−03
4 −5	1.50+00	5.25+00	1.48+00	6.42+00	1.38+00	1.38+01	1.21+00	3.14+01	1.05+00	3.82+01
4−6	1.57−01	8.40−01	1.51−01	8.34−01	1.27−01	1.13+00	8.28−02	1.67+00	3.24−02	1.99+00
4 −7	1.72−01	1.09+00	1.66−01	1.05+00	1.40−01	1.37+00	9.16−02	2.12+00	3.67−02	2.50+00
4−8	3.45−02	2.72−01	3.32−02	2.90−01	2.74−02	2.45−01	1.67−02	1.28−01	6.09−03	9.02−02
4−9	1.25−02	2.33−01	1.20−02	3.02−01	1.01−02	3.88−01	6.42−03	6.57−01	2.53−03	1.50+00
4 −10	3.15−02	2.79−01	3.05−02	5.28−01	2.59−02	2.16+00	1.70−02	1.04+01	6.73−03	1.32+01
4−11	2.44−02	4.72−01	2.37−02	4.81−01	2.02−02	3.08−01	1.34−02	2.09−01	5.33−03	3.29−01
4 −12	2.62−02	5.00−01	2.54−02	5.54−01	2.18−02	3.83−01	1.45−02	3.00−01	5.81−03	4.51−01
4−13	1.54−01	5.49−01	1.51−01	5.20−01	1.37−01	3.01−01	9.90−02	1.51−01	4.18−02	5.73−02
4 −14	1.20−01	6.35−01	1.18−01	6.03−01	1.06−01	3.28−01	7.60−02	1.50−01	3.20−02	5.54−02
4 −15	3.79+00	3.87+00	3.83+00	4.11+00	4.06+00	4.21+00	4.87+00	5.03+00	6.76+00	7.35+00
4 −16	1.01−01	8.36−01	1.00−01	4.98−01	9.80−02	2.83−01	9.32−02	1.74−01	9.90−02	1.31−01
4 −17	8.51−02	1.01+00	8.41−02	5.82−01	7.93−02	3.16−01	6.91−02	1.65−01	6.27−02	9.23−02
4 −18	5.63−02	1.02+00	5.48−02	5.91−01	4.77−02	3.14−01	3.24−02	1.36−01	1.29−02	3.93−02
4 −19	1.45−01	1.24+00	1.44−01	7.68−01	1.40−01	4.16−01	1.32−01	2.50−01	1.38−01	1.91−01
4 −20	4.54−02	3.76−01	4.48−02	2.84−01	4.18−02	1.37−01	3.35−02	6.56−02	2.15−02	2.99−02
4 −21	3.25−02	2.06−01	3.19−02	1.59−01	2.93−02	8.16−02	2.15−02	3.98−02	9.37−03	1.49−02

Table 7: Continued.

T_e(K)	7.20+03		3.60+04		1.80+05		7.20+05		3.60+05	
$i-k$	Present	BPRM	Present	BPRM	Present	BPRM	Present	BPRM	Present	BPRM
5−6	1.35−01	9.75−01	1.30−01	9.56−01	1.10−01	1.97+00	7.26−02	3.80+00	2.93−02	4.62+00
5 −7	3.67−01	1.94+00	3.54−01	1.91+00	2.99−01	2.51+00	1.96−01	4.13+00	7.94−02	5.03+00
5 −8	4.51−02	3.49−01	4.34−02	3.83−01	3.59−02	3.18−01	2.21−02	1.39−01	8.21−03	4.07−02
5 −9	3.57−02	2.85−01	3.45−02	3.35−01	2.92−02	2.93−01	1.90−02	2.45−01	7.46−03	2.21−01
5 −10	4.01−02	5.16−01	3.87−02	8.30−01	3.25−02	2.76+00	2.08−02	1.36+01	8.14−03	1.67+01
5 −11	2.28−02	5.12−01	2.21−02	5.19−01	1.90−02	3.78−01	1.27−02	4.36−01	5.08−03	9.30−01
5 −12	5.43−02	1.07+00	5.26−02	1.05+00	4.50−02	6.88−01	2.99−02	5.83−01	1.20−02	9.98−01
5 −13	5.89−02	1.07+00	5.75−02	1.05+00	5.10−02	6.88−01	3.59−02	5.83−01	1.52−02	9.98−01
5 −14	3.47−01	1.09+00	3.41−01	1.11+00	3.08−01	6.65−01	2.23−01	3.41−01	9.56−02	1.33−01
5 −15	5.64+00	5.85+00	5.70+00	6.18+00	6.05+00	6.33+00	7.28+00	7.58+00	1.01+01	1.11+01
5 −16	4.16−02	6.00−01	4.10−02	3.25−01	3.82−02	1.59−01	3.23−02	8.05−02	2.75−02	4.24−02
5 −17	1.02−01	1.03+00	1.01−01	6.26−01	9.67−02	3.39−01	8.77−02	1.90−01	8.58−02	1.21−01
5 −18	1.87−01	1.73+00	1.85−01	1.06+00	1.78−01	6.00−01	1.64−01	3.46−01	1.65−01	2.33−01
5 −19	2.42−01	2.66+00	2.39−01	1.59+00	2.27−01	8.99−01	1.99−01	4.80−01	1.84−01	2.86−01
5 −20	9.94−02	6.20−01	9.78−02	4.82−01	9.00−02	2.47−01	6.71−02	1.22−01	3.16−02	4.94−02
5 −21	2.21−02	2.31−01	2.17−02	1.73−01	1.97−02	8.39−02	1.43−02	3.70−02	6.00−03	1.21−02
6 −7	8.01−01	6.35+00	7.90−01	5.72+00	7.39−01	6.01+00	6.53−01	8.28+00	5.70−01	8.73+00
6 −8	6.16−01	9.76−01	6.11−01	1.15+00	5.93−01	1.02+00	5.86−01	8.22−01	6.14−01	7.83−01
6 −9	1.66−01	1.34+00	1.64−01	9.23−01	1.53−01	8.06−01	1.38−01	1.55+00	1.27−01	1.80+00
6 −10	1.65−01	1.08+00	1.60−01	1.06+00	1.38−01	1.60+00	9.85−02	6.56+00	5.39−02	9.22+00
6 −11	1.06−01	2.72+00	1.02−01	2.07+00	8.32−02	1.70+00	5.32−02	1.60+00	2.66−02	1.64+00
6 −12	1.53−01	1.60+00	1.47−01	1.26+00	1.18−01	1.04+00	7.20−02	1.26+00	3.35−02	1.48+00
6 −13	1.27+00	1.68+00	1.29+00	1.71+00	1.35+00	1.43+00	1.57+00	1.42+00	2.13+00	1.86+00
6 −14	2.95−01	1.04+00	2.94−01	1.10+00	2.90−01	6.59−01	2.90−01	3.93−01	3.22−01	3.18−01
6 −15	7.46−04	2.60−01	7.32−04	2.24−01	6.69−04	1.08−01	5.48−04	3.79−02	4.40−04	1.25−02
6 −16	1.68−01	6.18−01	1.64−01	4.75−01	1.47−01	2.84−01	1.05−01	1.53−01	4.59−02	5.92−02
6 −17	1.94−01	7.34−01	1.90−01	5.68−01	1.69−01	3.41−01	1.19−01	1.80−01	4.88−02	6.62−02
6 −18	1.52−01	6.70−01	1.49−01	4.97−01	1.32−01	2.90−01	9.32−02	1.50−01	3.81−02	5.23−02
6 −19	1.65−02	4.57−01	1.60−02	2.65−01	1.38−02	1.19−01	9.28−03	4.64−02	3.69−03	1.23−02
6 −20	4.62−01	1.01+00	4.66−01	8.37−01	4.86−01	6.36−01	5.70−01	6.14−01	7.76−01	8.10−01
6 −21	2.23+00	2.30+00	2.25+00	2.22+00	2.39+00	2.26+00	2.88+00	2.79+00	4.03+00	4.15+00

Table 8: Ratio of our effective collision strengths Υ (AS) to the BPRM [2] ones for some chosen forbidden transitions and their radiative decay rates.

Forbidden transitions			Allowed transitions		
$i-j$	$A_{ji}(s^{-1})$	AS/BPRM	$i-j$	$A_{ji}(s^{-1})$	AS/BPRM
1 – 17	1.991E−02	0.16	1 – 4	4.343E+03	0.29
3 – 6	1.211E−01	0.17	1 – 3	2.522E+05	0.37
1 – 16	2.945E+00	0.57	4 – 16	1.125E+06	0.43
6 – 8	4.969E+01	0.66	7 – 13	7.75E1+07	0.65
2 – 20	8.416E+04	0.95	1 – 11	1.651E+10	0.99

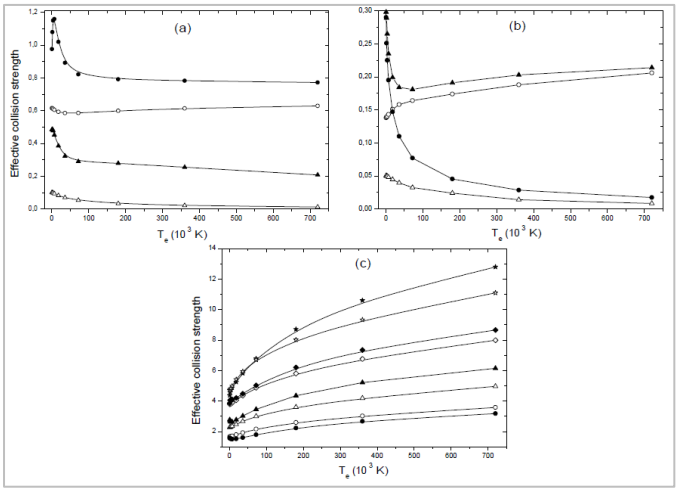

Figure 3: Effective collision strength Υ as a function of electron temperature T_e. Panel (a): the two forbidden transitions $3-6$ (△) and $6-8$ (∘). Panel (b): the two forbidden transitions $1-17$ (△) and $2-20$ (∘). Panel (c): the 4 electric dipole transitions 1 – 8 (∘), 1 − 9 (△), 1 − 11 (⋄) and 4 − 15 (⋆). Open symbols refer to our DW results and filled symbols to the BPRM ones [2].

4. Summary of the results and conclusion

Structure and collision calculations have been performed in the present work using the code AUTOSTRUCTURE [13]. We have used the 12 configurations: 3s ^{2}3p, 3s3p ^{2}, 3s ^{2}3d, 3p ^{3}, 3s3p3d, 3s ^{2}4s, 3s ^{2}4p, 3p ^{2}3d, 3s ^{2}4d, 3s3p4s, 3s3p4p and 3s3p4d yielding to 121 fine structure levels. Comparison of energy levels has been performed with the results of the multiconfiguration Hartree–Fock (MCHF) approach [8] and with the NIST values [11] for the lowest 60 levels. Agreement between the three results is about 3 % except for some levels belonging to the configuration 3s3p3d for which the difference reaches 5 %. We found disagreements in the term splitting energy between our results and those of MCHF and NIST. Lifetimes have also been reported. Radiative atomic data (line strengths, oscillator strengths and radiative decay rates) have been calculated for allowed (E1) transitions. We reported the results for transitions between the ground level and the lowest 43 ones. Comparisons for these allowed transitions have been performed with the calculations of [8]. The averaged difference between the two results was about 25 %, except transitions between the precedent levels which presented a high disagreement in their energies. Radiative decay rates and line strengths for forbidden electric quadrupole (E2), octopole (E3), magnetic dipole (M1) and quadrupole (M2) have been also provided. To the best of our knowledge, no other radiative data for forbidden transitions have been found in the literature, except the M1 transition 3s ^{2}3p ^{2}P$_{1/2}$ −3s ^{2}3p ^{2}P$^o_{3/2}$ (1−2) where it has been presented by NIST [11]. The agreement for this transition was good (about 2 %). Excitation collision strengths between fine structure levels have been calculated at electron energies 10, 50, 100, 200, 400 and 800 Ry. To our best knowledge, there are no collision strength data in the literature to compare with. We presented collision strengths for transitions from the levels $1-5$ to the levels $2-21$. We have used also the UCL codes SST/DW/JAJOM to provide collision strengths, and we have compared with the AS results for some selected transitions. In general, our collision strengths match the infinite energy Born limited except for some dipole electric transitions. We perform a study of collision strength convergence with the total angular momentum J. We showed that the convergence behaviour depends on the transition type, but in general our collision strengths converge even for (E1) transitions and at high electron energies. Effective collision strengths, which are very important in astrophysical applications, have been evaluated for an electron temperature ranging from 7.2×10^3 to 3.6×10^5. A detailed comparison has been performed between our results obtained from the code ADASEXJ (using our distorted wave collision strengths) and those of the BPRM method [2]. Several conclusions have been drawn from this comparison: our effective collision strengths are in good agreement with those of the BPRM method for allowed transitions, but for forbidden transitions, the agreement is less. The agreement increases also with the strength of the transition. We hope that our results for allowing and especially for forbidden transitions (missing in the literature) will be helpful for astrophysical and solar plasmas modelling.

Acknowledgements*:* This work has been supported by the Tunisian Laboratory of Molecular Spectroscopy and Dynamics LR18ES02.

Conflicts of Interest: Declare conflicts of interest or state "The author declares no conflict of interest."

References

[1] J. M. Munoz Burgos, C. P. Balance, S. D. Loch, R. F. Boivin. Electron-impact excitation of Ar $^{2+}$. *Astron. Astrophys.* **2009**, *500*, 1253-1261. 10.1051/0004-6361/200911743

[2] J. A. Ludlow, C. P. Ballance, S. D. Loch, F. S. Pindzola. Breit–Pauli R–matrix electron–impact excitation calculations along the argon isonuclear sequence. *J. Phys. B: At. Mol. Opt. Phys.* **2010**. *43*, 74029. 10.1088/0953-4075/43/7/074029

[3] T. Rauch, M. Ziegler, K. Werner,J. W. Kruk, C. M. Oliveira, D. Vande Putte, R. P. Mignani, F. Kerber. High-resolution FUSE and HST ultraviolet spectroscopy of the white dwarf central star of Sh 2–216. *Astron. Astrophys.* **2007**, *470*, 317-329. 10.1051/0004-6361:20077166

[4] L. W. Phillips, W. L. Parker. Spectra of Argon in the Extreme Ultraviolet. *Phys. Rev.* **1941**, *60*, 301-307. 10.1103/PhysRev.60.301

[5] M. Raineri *et al.* Revised and extended analysis of five times ionized argon (Ar VI). *Phys. Scr.* **1992**, *45*, 584-589. 10.1088/0031-8949/45/6/008

[6] M. Raineri, M. Gallardo, F. O. Borges, A. G. Trigueiros, J. Reyna Almandos. Extended analysis of the Al-like argon spectrum. *Phys. Scr.* **2009**, *79*, 25302. 10.1088/0031-8949/79/02/025302

[7] G. P. Gupta, A. Z. Msezane. Calculated Energy Levels, Oscillator Strengths and Lifetimes in Al-like Argon. Phys. Scr. **2004**, *69*, 273. 10.1238/Physica.Regular.069a00273

[8] C. Froese Fischer, G. Tachiev, A. Irimia. Relativistic energy levels, lifetimes, and transition probabilities for the sodium–like to argon–like sequences. At. Data Nucl. Data Tables. **2006**, *92*, 607-812. 10.1016/j.adt.2006.03.001

[9] J. Colgan, H. L. Zhang, C. J. Fontes. Electron-impact excitation and ionization cross sections for the Si, Cl, and Ar isonuclear sequences. *Phys. Rev. A.* **2008**, *77*, 62704. 10.1103/PhysRevA.77.062704

[10] H. Elabidi. Electron impact excitation for Ar VI. Journal of Physics: Conference Series. **2012**, *397*, 012055. 10.1088/1742-6596/397/1/012055

[11] A. Kramida, Yu. Ralchenko, J. Reader and NIST ASD Team. NIST Atomic Spectra Database (ver. 5.5.6), [Online]. Available: https://physics.nist.gov/asd. National Institute of Standards and Technology, Gaithersburg, MD. **2018**

[12] N. R. Badnell. On the effects of the two-body non-fine-structure operators of the Breit-Pauli Hamiltonian. *J. Phys. B: At. Mol. Opt. Phys.* **1997**, *30*, 1-11. 10.1088/0953-4075/30/1/005

[13] N. R. Badnell. A Breit–Pauli distorted wave implementation for AUTOSTRUCTURE. *Comput. Phys. Commun.* **2011**, *182*, 1528-1535. 10.1016/j.cpc.2011.03.023

[14] W. Eissner, M. Jones, H. Nussbaumer. Techniques for the calculation of atomic structures and radiative data including relativistic corrections. *Comput. Phys. Commun.* **1974**, *8*, 270-306. 10.1016/0010-4655(74)90019-8

[15] W. Eissner. The UCL distorted wave code. *Comput. Phys. Commun.* **1998**, *114*, 295-341. 10.1016/S0010-4655(98)00082-4

[16] H. E. Saraph. Fine structure cross sections from reactance matrices. *Comput. Phys. Commun.* **1972**, *3*, 256-268. 10.1016/0010-4655(72)90071-9

[17] H. E. Saraph. Fine structure cross sections from reactance matrices, a more versatile development of the program JAJOM. *Comput. Phys. Commun.* **1978**, *15*, 247-258. 10.1016/0010-4655(78)90095-4

[18] H. A. Bethe, E. E. Salpeter. Quantum Mechanics of One–and Two–Electron Atoms. Berlin, Göttingen: Springer, 1957

[19] R. D. Cowan, K. L. Andrew. Coupling Considerations in Two-Electron Spectra. *Journal of the Optical Society of America*. **1965**, *55*, 502-516.

[20] G. Racah. Theory of Complex Spectra. III. *Phys. Rev.* **1943**, *63*, 367-333. 10.1103/PhysRev.63.367

[21] A. Burgess, V. B. Sheorey. Electron impact excitation of the resonance lines of alkali-like positive ions. *J. Phys. B: At. Mol. Phys.* **1974**, *7*, 2403-2416. 10.1088/0022-3700/7/17/026

[22] A. Burgess, D. G. Hummer, J. A. Tully. Electron Impact Excitation of Positive Ions. *Philosophical Transactions of the Royal Society of London Series A.* **1970**, *266*, 225-279. 10.1098/rsta.1970.0007

[23] M. C. Chidichimo. S. P. Haigh. Electron-impact excitation of quadrupole-allowed transitions in positive ions. *Phys. Rev. A.* **1989**, *39*, 4991-4997. 10.1103/PhysRevA.39.4991

[24] M. C. Chidichimo. Electron-impact excitation of electric octupole transitions in positive ions: Asymptotic behavior of the sum over partial-collision strengths. *Phys. Rev. A.* **1992**, *45*, 1690-1700. 10.1103/PhysRevA.45.1690